N79-27806

A COMPARISON OF SIMULATED AND EXPERIMENTAL WAVE SPECTRA IN THE NEARSHORE REGION

by

W. Douglas Morris
B.S. July 1965, North Carolina State University

A Thesis Submitted to the Faculty of
Old Dominion University in Partial Fulfillment of the
Requirements for the Degree of

Master of Science

Oceanography

Old Dominion University
April, 1979

Approved by:

_____
Chester E. Grosch

_____

_____

ABSTRACT

A COMPARISON OF SIMULATED AND EXPERIMENTAL WAVE SPECTRA

IN THE NEARSHORE REGION

W. Douglas Morris
Old Dominion University, 1979
Director: Dr. Chester E. Grosch

The increasing use of the world's continental shelf and shoreline for resource, recreation, and commercial activity will require improved abilities to monitor and predict the wave climate of these areas for safe and efficient management of the nearshore region. For predictive models to be used in this process, they must first be verified by comparison with in situ wave measurements. This paper compares the wave energy spectra from one such model, with spectra from continuous wave height measurements of a wavefield moving from deepwater to the shoreline after passage of tropical storm Amy on July 2, 1975. Discussion of the theoretical model, data gathering techniques, historical development and the analysis procedures are also included.

The results of comparing the experimental spectra measured over the shelf with spectra measured in deepwater conditions indicated that statistically significant changes occurred over the shelf region that could be attributed to shoaling and refraction effects. The comparison of the simulated spectra with the experimental agreed well at the 80% confidence level for all but the most inshore data segment. The total energy also showed similar agreement, however, the theoretical frequency

at which peak spectral density occurred did not follow the decreasing trend seen in the experimental data. Guidelines are proposed for determining the type wavefield to which the modeling technique can best be applied, and caution is given on the selection of the digitization rate necessary to ensure sufficient detail for analysis of wave data.

ACKNOWLEDGEMENTS

I would like to thank the members of my thesis committee, Dr. C. E. Grosch, Dr. J. C. Ludwick and Dr. C. H. Blair, for their encouragement and guidance on this project. A special debt of gratitude is owed Mr. Lamont R. Poole, of the National Aeronautics and Space Administration, Langley Research Center, for frequent consultations and discussion of this research project.

TABLE OF CONTENTS

INTRODUCTION

The increasing use of satellites for synoptic monitoring of the ocean surface conditions will furnish information that can be used to better plan and utilize the nearshore regions. A combination of satellite sensors will measure wave height, direction, wind speed and provide data that can be used for the computation of wave spectra (McCandless, 1974). However, these measurements will represent a broad-scale look at the ocean surface in offshore areas where the surface conditions are relatively homogeneous over the swath coverage of the satellite. By using this data obtained from remote sensing in conjunction with theoretical computer modeling techniques, it should be possible to extend the useful range of the satellite data further into the coastal zone and to provide more detailed short-term predictions of the sea conditions in the nearshore region. One such technique requires only the initial deep-water wave height, direction and wave period for use in a linear wave refraction model to determine changes in wave characteristics as they propogate across the shelf. Such capabilities, when combined with satellite data would make possible an extended use of the satellite data in coastal zone planning and management, for such as coastal disaster warning, coastal protection and development, and offshore siting for facilities. Before such a modeling technique could be used as an operational management tool, the results of the model would have to be verified by comparison with measured ocean wave data.

The purpose of this research was to compare simulated wave energy spectra, with wave energy spectra from experimental data. The experimental

data were recorded off the coast of North Carolina on July 2, 1975, after passage of tropical storm Amy. Wave energy spectra were computed from the experimental data using the method of Blackman and Tukey (1958). The simulated spectra were estimated using a theoretical linear refraction computer model and a technique based on the method of Pierson, Neumann, and James (1955) for constructing wave spectra.

HISTORY AND RELATED WORK

As waves cross from deep water into shallow water their speed and direction change as an interaction occurs between the wave form and the sea floor. That portion of the wave which first encounters shallow water is slowed, while that portion that remains in deep water continues at a speed greater than the shallow water wave speed. This causes a bending and reshaping of the wave crest known as refraction. These changing wave patterns affect the distribution of wave energy over the shelf and along the shoreline.

Theoretical Models

Prediction models have been developed which, given deep water input parameters, can be used to determine these changes in wave energy. Early models such as that developed by Johnson and O'Brien (1946), used graphical construction of each wave crest as it advanced inshore. Later, this model was expanded to construct wave ray diagrams without drawing the wave crest (Johnson, O'Brien, and Issacs, 1948). This was still a graphical technique with the wave rays perpendicular to the wave crest. Graphical processes like these were later incorporated into computer programs by Griswold (1963), Mehr (1962), and Harrison and Wilson (1964), but these programs used a spatial grid of wave speeds to calculate the path of the wave ray and thus limited its usefulness by requiring a new grid for each new wave period. A newer model developed by Wilson (1966), eliminated many of the problems associated with the wave speed

grid by using a grid of water depths in computing wave ray position. Dobson (1967), combined wave ray construction using a grid of water depths with a finite-difference solution to the equations of wave intensity as developed by Munk and Arthur (1952), to compute wave height.

With the advent of the computerized refraction model, it became practical to compute the effects of refraction on ocean waves in the manner first proposed by Pierson, Newmann, and James (1955). Their theory called for the refraction of a large number of simple sine waves from various directions and with various periods about some point of interest in shallow water. From these results, plots could be constructed of two functions which show the variations in refraction and direction of waves about this location. The spectrum of the deepwater waves that would be refracted would then be divided into an approximating sum of simple sine waves, with a frequency, direction and a fraction of the total energy of the spectrum characterizing each sine wave. These values would then be used with the previously constructed refraction and direction charts to compute the incremental energy and direction at the point of interest for each deepwater sine wave. By then summing the results of each sine wave from the deepwater spectrum both the wave height and direction at the shallow water location could be determined. This is possible because theoretical considerations indicate that, even for spectral frequencies separated by only a small amount, the individual sine waves behave independently of each other as far as refraction is concerned. With modifications, this principle has been applied to

several recent papers. Chao (1974) used this technique to predict the refracted wave spectrum near the Chesapeake Bay entrance, and Poole (1976b) used this technique to compare remotely sensed wave spectra, with that computed using a wave refraction model similar to Dobson's.

Instrumentation

For a number of years oceanographers have been searching for ways to improve recordings of wave height distributions and a number of in situ instruments have been developed, but it was not until the early fifties that the first wave measurements were made from an aircraft using a wave profiling radar (Ross, Peloquin, and Sheil, 1968). Following the advent of lasers, the laser wave follower profilometer was developed in the late sixties (Ross, Peloquin and Shiel, 1968). The profilometer has since been used in other studies by Schule, Simpson and DeLeonibus (1971) and Poole, (1976b).

Experimental Analysis

Because of the random nature of ocean waves, a statistical approach is desirable in defining the properties of the sea surface. It was in 1952 that Pierson (See Kinsman, 1965), building on the theories of Tukey and Hamming (See Kinsman, 1965) on power spectra in the field of electronics, applied these theories to the study of ocean waves. Newmann (See Kinsman, 1965) applied the power spectrum theories to ocean wave time histories to obtain the wave energy spectrum as a function of mean wind. St. Denis and Pierson (1953) first addressed the problem of using

the spectrum of a wave record made from a moving platform and mapping this into its counterpart in a stationary reference frame. This spectrum is valid only in the moving reference frame, and thus gives a distorted estimate of what would be the true frequency estimate in the stationary reference frame. Cartwright (1963) used the theories discussed in St. Denis and Pierson to map the spectrum from the moving reference frame into its counterpart in a stationary reference frame. These transformation relationships were used in a study on wave generation by Barnett and Wilkenson (1967), Ross, Peloquen, and Shiel (1968) and Schule, Simpson, and De Leonibus (1971). These latter two reports used a laser profilometer to measure wave height histories where the first report used radar.

Poole (1976a) showed that the deep water approximation to the linear wave dispersion relationship, as had been previously used, introduced errors when applied in areas of shallow or intermediate water depths where refraction takes place. Poole developed transformation equations valid for all depth zones and used these in the study of a wave field (Poole, 1976b) where a comparison was made between remotely sensed wave spectra and spectra computed by using a wave refraction computer model. However, most of the energy of the wave field was at frequencies higher than the frequencies for which refraction was predicted. In addition, the variations among the remotely sensed spectra were statistically insignificant and thus the variation could not be attributed to any physical causes.

The present study was of a higher energy wave field associated with the passage of a tropical storm. The frequencies at which the energy would be concentrated could be expected to be those for which refraction effects would be predicted. In addition, longer wave lengths and periods associated with storm conditions would produce stronger shoaling and refraction effects which increase the likelihood of significant changes in the levels of the experimental spectra. For these reasons, the methods employed in Poole (1976b) were applied to the wave data from tropical storm Amy.

GOVERNING EQUATIONS

Wave energy spectra is a measure of the energy distribution with frequency. Changes in the spectral shape are indicative of a shifting of the wave energies to different frequency bands. As waves cross the shelf region the change in spectral shape can be used to compare the redistribution of the wave energy. The spectra can be computed either from measured wave heights or from the results of a wave refraction model. The equations governing the computation of energy spectra are presented as follows:

Spectra from Measured Data

The energy in the ocean waves is a function of the fluctuations in water height. This fluctuation is a random process and as such is describable by the laws of probability. In order to generate a wave energy spectrum from records of finite length, it is necessary to assume that the process is both stationary and ergodic (Kinsman, 1965). Using a time history of the surface elevation variation about the mean, a wave spectrum can be computed by first taking the autocorrelation of the data record. The autocorrelation function is a measure of the degree of parallelism between a given time series $\eta(t)$ and the same series at a displacement τ. From Bath (1974), the autocorrelation is computed by

$$C(\tau) = \frac{1}{N-\tau} \sum_{t=1}^{N-\tau} \eta(t)\eta(t+\tau) \qquad (1)$$

$$\tau = 0,1,2,\ldots M$$

where M is the maximum number of lags.

The raw spectral density estimates are then computed by taking the Fourier transform of the autocorrelation function using the following equation:

$$S_\ell = \frac{1}{M}\left[C(0) + 2 \sum_{\tau=1}^{M-1} C(\tau) \cos \frac{\ell\pi\tau}{M} + C(M) \cos \ell\pi \right] \qquad (2)$$

which divides the spectra into M frequency bins of equal width ($1/2\ \Delta t$). In transforming the autocorrelation function, these data have in effect been passed through a lag window (Båth, 1974) and the undesirable spectral effects which are thus introduced are then compensated for by smoothing in the frequency domain. The smoothed spectral density estimates are obtained by applying the Hamming-Tukey smoothing equation to equation (2).

$$\bar{S}_\ell = .23S(\ell - 1) + .54S(\ell) + .23S(\ell + 1) \qquad (3)$$

These spectral density estimates represent the one-side cosine transform values.

In the case where the data are recorded in a moving reference frame, the frequency is shifted from that which would be seen in a fixed reference frame. In this case, the frequency associated with each spectral bin ℓ, represents an apparent frequency as seen from the moving platform. In order to map the apparent spectrum into a stationary reference frame, the unidirectional transformation technique developed

by Poole (1976a) is used. This technique utilizes the fact that an equivalent amount of energy density must reside in both the apparent frequency bin and the transformed frequency bin. In the stationary reference frame, the width of the frequency bins vary, and the corresponding spectral densities must also change to maintain a constant amount of energy density. Thus the transformation is made in pairs, such that for each apparent frequency and spectral density pair in the moving reference frame, there will be a corresponding frequency and spectral density pair in the stationary reference frame. The transformation uses specific values of aircraft velocity, apparent frequency, and averaged water depth for the region of study, to find a unique iterative solution for the wave number k (equation 4) under the assumption that the speed of the platform from which the measurements were made was

$$\underline{kV} - (gk \tanh k\bar{d})^{1/2} - \omega_a = 0 \qquad (4)$$

greater than the speed of the fastest wave. The corresponding frequency and spectral density can then be computed in the stationary reference frame by using equations (5) and (6)

$$\omega^2 = gk \tanh k\bar{d} \qquad (5)$$

$$S(\omega) = S_a(\omega_a)\left(\frac{2\omega\, V/g}{\tanh k\bar{d} + k\bar{d}\,\operatorname{sech}^2 k\bar{d}}\right) \qquad (6)$$

Simulated Spectra

Wave energy spectra can be constructed using wave refraction models as discussed in Pierson, Neumann, and James (1955), Chao (1974), and Poole (1976b). These refraction models predict the changing wave characteristics and crest patterns produced by waves as they interact with the bottom topography (Goldsmith, et al. 1974). As the waves move from deep water into shallower water, the wave speed is slowed and the wave shape becomes shorter and steeper. Since the process is not uniform, but varies with the changing depths, the varying wave speed along the crest causes the bending of the wave front. This process is analogous to the refraction of light rays in optics and is governed by Snell's law:

$$\frac{\sin \alpha_2}{\sin \alpha_1} = \frac{c_2}{c_1} \tag{7}$$

where α_1, and α_2 are the angles between successive wave fronts and the corresponding bottom contours as shown in the accompanying sketch, and c_1 and c_2 are the respective wave celerities associated with these wave fronts. Assuming steady state conditions and a progressive sinusoidal wave with small steepness and constant frequency, linear wave

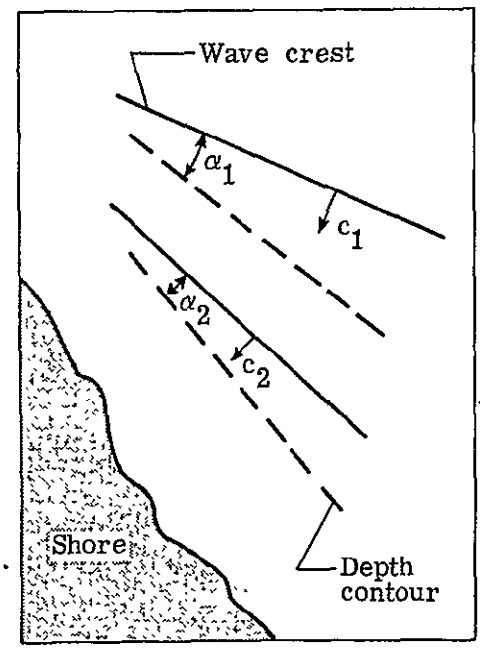

theory can be used to compute the local wave celerity from the dispersion relationship

$$c^2 = \frac{gL}{2\pi} \tanh \frac{2\pi d}{L} \quad . \tag{8}$$

Using a deepwater direction and period, the local phase speed and wave curvature can be computed. These values are then used to compute a new phase speed and curvature for the next point at some fixed time step and by this means the wave pattern is advanced shoreward. For a more detailed discussion of this technique see Dobson (1967), Goldsmith, et al. (1974), and Poole, et al. (1977).

The result of refraction is to change wave height as well as wave direction. By assuming that no energy flows laterally along the wave crest, and that no energy is gained or lost due to reflection, percolation, or bottom friction, then the wave height can be determined from,

$$\frac{H}{H_o} = K_r K_s \tag{9}$$

where K_r is the refraction coefficient,

$$K_r = \left(\frac{b_o}{b}\right)^{1/2} \tag{10}$$

and K_s is the shoaling coefficient

$$K_s = \left(\frac{2 \cosh^2 kd}{2kd + \sinh kd} \right) \tag{11}$$

Since the wave energy is proportional to the square of the wave height, equation (9) can be used to compute a normalized energy amplification function as follows:

$$\bar{F}(f) = \frac{E(f)}{E_o(f)} = K_r^2(f)\, K_s^2(f) \ . \tag{12}$$

The amplification function $\bar{F}(f)$, is computed for the full frequency range corresponding to each spectral region using the refraction model to compute the refraction and shoaling coefficients for the monochromatic wave frequencies of the reference spectrum. Combining these values with the spectral densities of the reference spectrum $S_o(f)$, the inshore simulated spectra can then be determined from equation (13) as a function of wave frequency (Poole, 1976b).

$$S(f) = S_o(f)\, \bar{F}(f) \tag{13}$$

PROCEDURES

Data Collection

The wave data used in this study are from wave measurements taken on July 2, 1975, after passage of tropical storm Amy off the coast of North Carolina. At the time of the experiment (1600-1630 d.s.t.) Amy's storm center was approximately 512 n.mi. offshore and had maximum sustained winds of 60 knots. The ground track of the storm is presented in figure 1, and position data in table 1. During the 48 hour period prior to the data gathering flight, the storm moved further out to sea in a relatively constant direction from the test site. Figure 2 is a photograph from the Synchronous Meteorological Satellite-1 (SMS-1) showing the position and size of the storm near flight time.

Data were taken as a part of a flight experiment using a NASA C-54 aircraft stationed at Wallops Island, Virginia. The data leg (see sketch) began approximately 81 n.mi. offshore at an altitude of 152 meters and flown in the onshore direction along the path of swell propagation, as determined from preflight wave reports and visual observation from the aircraft. A continuous surface profile was measured along

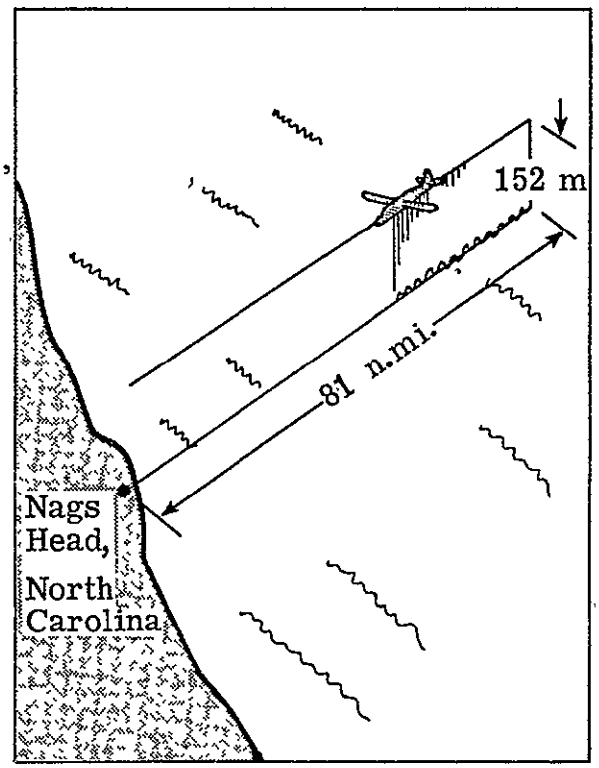

this line of flight using a laser wave profilometer and recorded on analog tape. Data gathering was terminated at the shoreline over Jennette's Pier, Nags Head, North Carolina. An inertial navigation system was used to periodically record the flight position as presented in figure 3. Visibility was 7 miles or better in the experimental area with little cloudiness. Surface winds were from the Northwest at 5 to 10 knots.

The laser profilometer used to record the wave height time history was furnished and operated by the Naval Oceanographic Office (NOO). The instrument was a Spectra Physics Geodolite-3 ranging system utilizing a constant wavelength helium-neon laser with a wavelength of 632.8 nm, and had an output of 25 millivolts (Ross, Peloquin, and Shiel, 1968).

Experimental Analysis

The surface elevation time history was recorded and preprocessed by the NOO. Raw data were measured by a laser profilometer and recorded as an analog signal. This record was then digitized at a 0.02 second interval and divided into 10 consecutive data segments. From the offshore position, the first nine segments were each 3 minutes (9000 samples) long and the tenth was 1.727 minutes (5181 samples) long. The 10th segment was shorter as the data record was terminated at the beach. Thus 10 quasi-homogeneous data sets were available for analysis. Data were recorded in terms of voltage and converted to altitude measurements by using an NOO supplied data factor. A Linette high pass filter (Linette, 1961) was used to remove low frequency (less than 0.15 hertz)

aircraft vertical motions from the data. Roll and pitch motions were assumed to have a negligible effect on the data record when an aircraft of this size is used (Barnett and Wilkerson, 1967).

For each data segment, the mean surface elevation was computed and subtracted from the data record. Subsequent computations were based on wave fluctions about the mean as it is the variability of the fluctuations which is the statistically stable quantity to be examined (Kinsman, 1965). The data record then represented surface elevation variations with time in the aircraft reference frame. This moving reference frame provided a compressed data record from that which would be observed in a stationary reference frame. This apparent wave spectrum was first computed and then transformed into the stationary reference frame to obtain the experimental spectrum.

The apparent spectrum was computed using the autocorrelation function in equation (1) for each data segment. The number of lags M for this equation must be chosen as a compromise between the desired degree of correlation stability and spectral resolution. A large value of M increases the resolution but decreases the number of terms used to compute the correlation which might lead to fluctuations in the values of the autocorrelation functions. Blackman and Tukey (1958) recommend that M be no more than 5 to 10 percent of N for power spectrum computations, but aside from this restriction the value used becomes a matter of judgment. Figure 4 shows the autocorrelation as a function of τ for 150 lags. For most spectra this represents 114 degrees of freedom. No further significant changes in the autocorrelation

function was seen when larger values of M were tried. The Fourier cosine transform of this autocorrelation function was then used to compute the raw power spectrum according to equation (2), and the values then smoothed by the Hamming-Tukey equation (3). Then these smoothed apparent spectral values were transformed to the stationary reference frame by using the unidirectional transformation technique in equations (4), (5) and (6). The apparent frequency values were calculated from the raw data, the aircraft velocity was 83.8 m/s and the average depth was determined by averaging the depth along the flight line for each segment. The resulting experimental wave spectra in the stationary reference frame are presented in figure 5 for the first 4 data segments. Since these first 4 spectra are each from measurements made under similar deepwater conditions, they may be regarded as statistically independent random variables and can be added together to improve the accuracy and statistical stability of the resultant spectrum (Lumley and Panofsky, 1964). This is then known as the deepwater reference spectrum and is presented in figure 6. The remaining 6 inshore experimental spectra are presented in figure 7.

Theoretical Analysis

A modified wave refraction computer program was used to construct the refraction diagrams used in calculating the simulated spectra. This program computes the wave orthogonals (perpendicular to the wave crest) based upon the analogy with Snell's law for optics given in equation (7). The program was modified (Poole 1976b) to initiate

ray computations at deepwater locations lying along a line perpendicular to the initial ray direction. (For this model, deepwater was considered when the local water depth was greater than 1/4 the wave length.) All computations were performed at fixed time increments referenced to the same initial time. A small family of wave rays were used, clustered about the initial wave ray and spaced 1 nautical mile apart. The initial ray was chosen to correspond closely with the data flightline which lies along the direction of wave propagation. Based on a least squares fit to the inertial navigation data, this angle was 59° as measured from true North. In the model coordinate system this is the angle between the flight track and the X-axis (Figure 8a). Refraction diagrams were computed for wave periods ranging from 6 to 14 seconds. There was negligible refraction for periods of less than 6 seconds and little energy associated with periods greater than 14 seconds, based on examination of the reference spectrum. Sample refraction diagrams are presented in figure 8 for wave periods of 6, 8, 10, 12 and 14 seconds. The circular symbols on each figure indicate the position of the inertial navigation points.

These diagrams were then used to compute the energy amplification function for each data segment. The normalized energy amplification function was computed from equation (11) for each ray pair that bounded the flight path. These values were then averaged over the flight path for each data segment. When more than one pair of rays bounded the flight path, weighted averages were used. For amplification values corresponding to frequencies higher than 0.167 hertz

(6 second period) the amplification value was assumed to be equal to 1 since no refraction takes place. For frequencies less than 0.071 hertz (14 second period) the amplification function was set at the value corresponding to 0.071 hertz. These normalized energy amplification functions are presented in figure 9 as a function of frequency for each data segment 5 through 10.

Simulated refracted spectra were computed by multiplying the deepwater reference spectrum (figure 6) by the energy amplification function according to equation (13), for each data segment 5 through 10. The resulting simulated spectra are presented in figure 10.

RESULTS AND DISCUSSION

In figure 11, the deep water sea state at the time of the experiment is compared with data from Phillips (1968, page 113, figure 4.8) for a fully developed sea and with the deepwater reference spectrum from Poole (1976b). The wave field associated with the passage of tropical storm Amy contained a significant portion of wave energy at frequencies lower than that measured by Poole, and an order of magnitude higher in spectral density. The reference spectrum for the Amy study (from figure 6) is for an area nearly 400 nmi from the center of the storm, but prior to the region of shoaling and refraction effects that occur further inshore. The data from Phillips illustrates the equilibrium range of the frequency spectrum for wind generated waves. The slope of the spectral peak is shown for only three cases in addition to the deepwater reference spectra; otherwise only the saturated part of each spectrum is shown. For the fully developed sea in figure 11, each possible frequency band in the spectrum is present with a maximum amount of spectral energy (Pierson, Neumann, and James, 1955, page 41). The shape of the reference spectrum does not match that for the fully developed sea, as would be expected since the reference spectrum is not in the generating area. At this distance from the storm, the waves have been filtered, with the longer waves (lower frequencies) arriving at this location before the shorter waves (higher frequencies) that were generated at the same time. Thus the reference spectrum with which the inshore spectra are compared

is based on a sea state that is not fully developed but is characteristic of the filtered sea that is outside the storm area.

The deepwater reference spectrum, figure 6, is the result of averaging the first four deepwater spectra to obtain a greater degree of statistical stability than the individual spectrum would have. The number of degrees of freedom goes from 114 for the individual spectrum to 458 for the combined reference spectrum and narrows the width of the confidence bands associated with the data. These bands imply that for repeated tests, the spectral density values would lie between 0.9016 and 1.086 times the values of the reference spectrum 80 percent of the time. Changes of the spectral levels that fall within these limits can be attributed to random fluctuations in the data, but changes which fall outside these values are due to either shoaling or refraction or a combination of these effects. Each of these factors effect the energy density levels by their effect on wave height according to equation (9). The experimental and simulated spectra are compared with the reference spectrum in figures 7 and 10, and with each other in figure 12.

In figure 7, the experimental spectra show a gradual decrease in the peak spectral density levels to a minimum in segment 7 (figure 7c) and rises again to a maximum in segment 9 (figure 7e) then drops rapidly to its lowest level in the most inshore segment, segment 10 (figure 7f). Segment 10 is also double peaked. The experimental spectra are further characterized by a shift of the frequency at which the peak energy density occurs to lower frequency levels as the spectra move shoreward. It is in spectral segments 7, 8 and 10 (figures 7c, 7d, 7f) that variations in

the data occur that exceed the 80 percent confidence bands of the reference spectrum and can be attributed to the effects of shoaling and/or refraction and not random fluctuations in the data.

In figure 10 the simulated spectra are compared with the reference spectrum. The peak spectral density level shows a general decrease to a minimum in spectral segment 8 (figure 10d), increases to a value greater than the reference spectrum in segment 9 (figure 10e) and then has a slight decrease in segment 10 (figure 10f). The spectrum becomes double peaked in segment 8 (figure 10d) and indicates a shift in the frequency of peak spectral density to a lower frequency in segment 10 (figure 10f). Even though this fits the general description of the experimental spectra, it is only in spectral segment 8 (figure 10d) that the change is sufficiently large to fall outside the 80 percent confidence bounds and would predict changes which could be considered statistically significant.

In figure 12, the simulated spectra are compared with the experimental spectra. Both show the same undulating variation in peak spectral values with a minimum near segments 7 and 8, rising again in segment 9 and decreasing again in segment 10. The overlapping confidence bands in all cases except segment 10 indicate good agreement between the simulated and experimental spectra for all but the most inshore segment. In figure 13 the total energies are compared and as in the spectral comparisons, the energy levels of the simulated spectra follow the general trend of the experimental total energies. A comparison is made of the frequencies at which the peak spectral density occurs in figure 14. There is a general

decrease in the experimental value from 0.1062 hertz (9.42 second period) in the reference spectrum to 0.0912 hertz (10.96 second period) in spectral segment 9. This shifting of the peak wave energies toward the lower frequencies (longer wave periods) as the waves move inshore was not duplicated by the simulated spectra. With this exception, the theoretical technique described in Poole (1976b), when applied to the data from tropical storm Amy was able to simulate the changes in the spectra caused by shoaling and refraction over most of the shelf area.

An examination of the behavior of the shoaling and refraction coefficients over the test region may help to understand the observed spectral changes in the wave field as it moves shoreward. The variation of the shoaling coefficient with bottom depth, as shown in Kinsman (1965, page 159) for the wave frequencies and depths associated with the test indicate that the shoaling coefficients for the first 9 segments were all less than 1. The effect of this coefficient is to decrease the spectral density as the wave field moves inshore, reaching a minimum value near spectral segments 8 and 9. Only in segment 10 would the shoaling cause an increase in the spectral density levels. Therefore, any increase in energy levels in the first 9 segments higher than the reference level would have to be due to the effects of the refraction coefficient. This value is dependent on the separation of wave rays that bracket the data segment and can have values which range from less than 1 for diverging rays to greater than 1 for converging rays. The energy amplification function shown in figure 9 best illustrates the combined effect of the shoaling and refraction coefficients in shifting the energy

density levels as the wave field moves inshore. After an initial reduction in values (seen in figures 9a and 9b) for the two most offshore segments (segments 5 and 6) there appears to be a general increase in the amplification function for lower frequency waves as the spectral segments move shoreward. This would be as expected since the longer waves (i.e., lower frequency waves) are the first to be affected by the bottom and show signs of shoaling and refraction. As the wave field moves inshore these effects spread toward the shorter waves (i.e., higher frequency waves) which also begin to be affected by the bottom and this shoreward progress can be observed in the amplification function. These observations are consistent with the shift of energy to lower frequencies seen in figure 7 for the experimental spectra, to a lesser degree in figure 10 for the simulated spectra and with the shift of the frequency of peak energy density shown in figure 14.

The spectra of segment 10 are unique relative to the spectra of the other data segments. The experimental spectrum is based on only slightly over half the total number of data points that were available for the offshore spectra, and about 8 percent of these were taken through the surf zone. The assumption of homogeneous wave conditions is also probably violated to some degree in this region as this is the area of maximum changes in the waves due to shoaling and refraction effects. For these reasons, the resulting spectra might be expected to show some anomolies. Yet the double peaked nature of the experimental spectrum is similar to the spectra recorded by the U.S. Army Corp of Engineers Research Center's (CERC) shoreline gauge located at Jennette's Pier,

Nags Head, North Carolina (Harris, 1975), and shown in figure 15. The experimental flight was coordinated with CERC personnel and was designed to pass directly over the recording station. The CERC spectra were generated from data recorded before, during, and after the flight passed overhead. Spectra 15b and 15c bracket the overflight. Nearly all the spectra have similar double peaks with the major peak near 0.08 hertz and the secondary peak near 0.15 hertz. This compares with 0.085 hertz and 0.153 hertz, respectively, for the experimental spectrum. As an indication of total energy, a significant wave height of 1.58m was computed from the experimental spectrum by trapezoidal integration of the area under the curve (under the assumption of a Guassian distribution of wave height). This compares well with the 1.86m and 1.74m for the CERC spectra nearest to flight time. Even though measured by two different techniques, the experimental spectra and the CERC spectra have similar characteristics. This would appear then to be an accurate description of the energy distribution in the most inshore area.

The secondary peaks observed in the segment 10 spectra, and not the offshore spectra, appear to be caused by nonlinear effects. In the rapidly shoaling waters just off the beach, the distortion of the wave form and the increase in wave height due to convergence creates nonlinear changes in the phase speed which are not of as large a magnitude in the deeper offshore waters (Grosch and Comery, 1977). In nonlinear wave theory these changes increase the terms which are direct multiples of the wave frequency (Grosch, 1978). In the experimental spectrum of segment 10, the secondary peak is at a frequency nearly double that of the primary

peak frequency. In the CERC spectra shown in figure 15d, peaks can be seen which correspond to multiples of 2, 3, and 4 times the primary peak frequency.

Although the experimental spectra from the aircraft data compared well with the CERC spectra, the simulated spectra failed to match this distribution (figure 12f). The significant wave height of 1.79m compares well with 1.70m for the experimental spectrum, but the simulated spectrum is single peaked, and at a much higher level of energy density. In this region of high wave activity, a number of assumptions on which the simulated spectra are based begin to fail. The small amplitude assumption requires wave height to be small relative to wave length and water depth (Kinsman 1965, p125) but in the shoaling water the wave lengths shorten and wave height increases: Also the equations used to compute refraction are strictly valid only for a constant water depth but have been used successfully in areas with a mild slope (Dobson, 1967). In segment 10, since the depth goes to 0, the slope can no longer be considered mild. For these reasons, the simulated spectrum might not be expected to match the experimental results.

It is an assumption of wave refraction theory that the energy between wave rays remains constant and does not cross the ray boundaries. Thus when rays diverge, the energy density decreases, and when they converge, the density increases. If the wave rays cross, a "caustic" is formed, indicating that the waves in this region have become so high as to be unstable and are breaking (Kinsman 1965, p 158). The practical application of this theory requires a decision on how to treat the energy

associated with the wave rays which formed the "caustic". In most of the offshore spectral segments, few rays crossed, and the energy from these rays was included in the calculation. The spectra in data segment 10 (figure 10f and 12f) were also computed in this manner. However, since in segment 10 there were many "caustics", this spectrum was also computed by a second method in which the energy from the crossed rays was not included in the computations. The results of this method are shown in figure 16. The simulated spectrum using this technique becomes double peaked and provided a better match with the experimental spectra than did the standard technique. For the same reasons that figure 12f did not match the experimental results, figure 16 should not either, but did. Whether this is a technique that better simulates the loss of energy due to wave breaking in this region, or simply a fortuitous result cannot be assessed from this single sample. That assessment will await repeated tests and is presented here as a point of interest for future work in this area.

Had the wave pattern displayed a more clearly defined direction of swell propogation or had there been only a single well defined swell, the overall comparison between the simulated and experimental spectra would possibly have been improved. Such a condition would better match the monochromatic conditions assumed in the theoretical model, and the assumption of wave movement along the flight path, than did the conditions measured. Photographs from the flight (Morris 1978) show a number of wave patterns propogating from the general direction of the storm. Even though there appears to be a slight dominance of the off flightline waves,

this could be attributed to the sun angle highlighting the photographs. The initial flight angle was chosen by visual observation from the aircraft at flight time, and even though a wave pattern similar to that seen in the post flight photographs was observed, the dominant direction used in the refraction model was the direction chosen for the flight path.

The local surface winds which were present were approximately perpendicular to the flightline and would not have greatly influenced the wave measurements along the direction of flight.

The amplification function curve for each spectral segment was constructed from over 20 sets of refraction diagrams to ensure that each major fluctuation in the curve was included. This is more detail than the modeling technique requires. The model computes the values of simulated spectral density for the frequencies which correspond to those from the reference spectrum (such as those shown by the arrows located along the abscissa of figure-9d). It is clear that much activity can occur between these points and will not be treated by the model, especially at the lower frequencies. As long as the computational points follow the general trend of the amplification function, the results would appear to be representative. In cases where the energy spectrum is spread over a broad frequency range, and where lower total energy is reflected in a less active amplification function, the modeling technique would not be overly sensitive to the location of the computational points. As energy concentrates toward the lower frequency range, however, the model will attempt to define the increasing concentrations of energy with a decreasing number of points. To increase the number of frequencies used in this

model, the digitization rate will have to be increased as this will better define both the reference spectrum and the simulated spectra. It should be noted that this can cause large increases in the model's computer requirements.

Although the data sampled does not represent the ideal conditions required for verification of the theoretical modeling technique, the wave climate is probably typical of the conditions for which it can be used. The study by Poole (1976b), illustrated in figure 11, apparently represents a minimum sea condition for which the model can be applied. The present study, with more energy at the lower frequency has established a level at which the model shows a sensitivity to the shoaling and refraction effects which are recognizable from the random fluctuations of wave energies. Studies of wave conditions which fall within the bounds established by the fully developed sea and the present study should help further establish the degree to which the model is sensitive to these changes.

CONCLUDING REMARKS

This report presents a comparison of simulated wave spectra with experimental wave spectra. Experimental spectra were computed from surface elevation measurements taken from an aircraft over the continental shelf region off North Carolina after passage of tropical storm Amy on July 2, 1975. Simulated spectra corresponding to 6 of the experimental spectral data segments were computed using a modified linear wave refraction model.

Conclusions

The deep water wave field associated with tropical storm Amy was not that of a fully developed sea, but probably typical of a wave field outside the wave generating area. High frequency waves had been filtered and energy concentrated toward the low frequencies. When compared with the spectrum of the deepwater wave field, the inshore experimental spectra showed a statistically significant change in spectral levels for several of the inshore spectra which can be attributed to shoaling and refraction effects. The spectra also showed a consistent shift of energy toward the lower frequencies as the wave field moved shoreward. The most inshore spectra agreed with the results of CERC shoreline spectra recorded simultaneous to the experiment. The simulated spectra followed the shift in energy levels of the experimental spectra for all but the most inshore spectral segment. The total energy levels were within 20 percent of the experimental levels but the shift in frequency of peak spectral density was not predicted by the simulated spectra.

Given a deepwater spectrum, the theoretical techniques used to simulate the spectra over the shelf appears to be capable of predicting the changes in spectral shape and energy levels that occur due to shoaling and refraction effects to within 5 nmi of the shoreline. Shoreward of this region the simulation technique fails to match the energy distribution of the experimental spectrum. Future applications of this technique for higher energy levels, will require careful selection of the rate at which the data is digitized to ensure a sufficient definition of the experimental spectra and to ensure the ability of the theoretical modeling technique to simulate the changes due to shoaling and refraction effects.

Suggestions for Future Work

1. Storm systems stronger than Amy will produce wave fields of even more interest to those concerned with wave energy distributions in the inshore area. The results presented in this report indicate the ability of the model to simulate the inshore spectra for a moderately strong storm such as Amy, but results will be needed from systems concentrating even higher energy levels to help determine the sensitivity of the modeling technique. The spectral comparison with fully developed sea spectra (figure 11) establishes bounds that can be used in evaluating the value of using a deepwater spectrum for simulation.
2. An assumption of the technique used to determine the experimental spectra is that the data is gathered along the direction of swell propogation. This is difficult to determine while observing the sea from an

aircraft and forecast wind information is often used to determine the flight direction. A comparison of spectra from data collected from several flight directions for the same wave field would help determine the sensitivity of the technique to errors in choosing the direction of swell propagation.

3. One impediment to the use of this theoretical technique to simulate the spectra is in determining the amplification factors for each spectral segment. The present system requires the use of an overlay to determine which ray pairs bracket the flight path and the manual summing and averaging of the amplification functions associated with these rays. This is a most tedious job and an obstacle to rapid application of this technique. The procedure should lend itself to at least partial automation which would greatly enhance the application of this technique and promote its use.

4. Although the method for simulating spectra predicts the energy distributions across the shelf, it fails in the most inshore case where there is frequencly even more need for the results. On the assumption that the wave conditions just offshore are indicative of the conditions at the beach, it should be of interest to see just how near to the surf zone the spectral segment can be extended and still simulate the experimental spectra. In the present case the simulation matches to within 4.7nmi of the beach. By selectively breaking the spectral segment to form a moving spectral band it should be possible to determine how far inshore the segment could be extended before failing. The nearer to shore the spectra matched, the higher would be the confidence that the

results would indicate conditions along the beach.

5. The technique described in this report, which excludes from the most inshore spectra the energy of those waves which crossed and formed a "caustic", should be explored. The uniqueness of this result can only be verified by application to another independent set of data. If the result is other than chance, the techniques would offer a method of extending the simulated spectra close to the shoreline.

REFERENCES CITED

Barnett, T.P. and Wilkerson, J.C. 1967. On the generation of ocean wind waves as inferred from airborne radar measurements of fetch-limited spectra. J. Mar. Res., vol. 25, no. 3.

Båth, M. 1974. Spectral analysis in geophysics. Elsevier Scientific Publishing Company, Amsterdam, The Netherlands. 563 pp.

Blackman, R.B. and Tukey, J.W. 1958. The measurement of power spectra. Dover Publications, Inc. 190 pp.

Cartwright, D.E. 1963. The use of directional spectra in studying the output of a wave recorder on a moving ship. in Proceedings of a Conference on Ocean Wave Spectra. Easton, Maryland: Prentice-Hall, Inc. 357pp.

Chao, Y.Y. 1974. Wave refraction phenomena over the continental shelf near the Chesapeake Bay entrance. Coastal Engineering research center, Tech. Memo 1647, Army Corps of Eng. 53 pp.

Dobson, R.S. 1967. Some applications of a digital computer to hydraulic engineering problems. Tech. Rep. No. 80, Dept of Civil Eng., Stanford Univ.

Goldsmith, V., Morris, W.D., Byrne, R.J., and Whitlock, C.H. 1974. Wave climate model of the mid-Atlantic shelf and shoreline (Virginian Sea), NASA SP-358.

Griswold, G.M. 1963. Numerical calculation of wave refraction. J. Geophys. Res., 68(6):1715-1723.

Grosch, C.E. 1978. Professor of Oceanography Institute of Oceanography, Old Dominion University. Personal communication, Norfolk, Virginia, 1973-1978 various.

Grosch, C.E. and Comely, W.J. 1977. Finite amplitude wave refraction, Tech. Rep. No. 34, Old Dominion University.

Harris, D.L. 1975. Chief, Oceanography Branch, Research Division, Coastal Engineering Research Center, Personal Communication.

Harrison, W. and Wilson, W.S. 1964. Development of a method for numerical calculation of wave refraction. Coastal Eng. Res. Center, Tech. Memo No. 6, Army Corps Eng. 64pp.

Kinsman, B. 1965. Wind Waves, their generation and propogation on the ocean surface. Prentice-Hall, Inc. Englewood Cliffs, New Jersey. 676pp.

Johnson, J.W. and O'Brien, M.P. 1946. Graphical construction of wave refraction diagrams, Univ. of Calif. Fluid Mechanics Lab., Tech. Rep. No. HE-116-221.

Johnson, J.W., O'Brien, N.P. and Isaccs, J.O. 1948. Graphical construction of wave refraction diagrams, U.S. Navy Dept, Hydrographic Office, Pub. No. 605.

Lumley, J.L. and Panofsky, H.A. 1964. The structure of atmospheric turbulence. Interscience Publishers. 239pp.

Linnette, H.M. 1961. Statistical filters for smoothing and filtering equally spaced data. U.S. Navy Electronics Laboratory, San Diego, California, Research Report 1049.

McCandless, S.W., Jr. 1974. SEASAT-A- A user oriented system design. Proceedings of the International Symposium on Applications of Marine Geodesy. Marine Technology Society, pp 67-74.

Mehr, E. 1962. Surf refraction: Computer refraction program, Tech. Rep. No. NWRE 36-0962-065, New York University.

Morris, W.D. 1977. Coastal wave measurements during passage of tropical storm Amy, NASA TM-74060.

Munk, W.H. and Arthur, R.S. 1952. Wave intensity along a refracted ray in Gravity Waves, Nat. Bureau of Standards Circular 521, pp 95-108.

Pierson, W.J.Jr., Neumann, G., and James, K.W. 1955. Practical methods for observing and forecasting ocean waves by means of wave spectra and statistics. U.S. Navy Hydrographic Office, Pub. No. 603 (reprinted 1960) 284 pp.

Phillips, O.M. 1969. The dynamics of the upper ocean. Cambridge University Press, London. 261pp.

Poole, L.R. 1976a. Transformation of apparent ocean wave spectra observed from an aircraft sensor platform. NASA TN D-8246.

Poole, L.R. 1976b. Comparison of remotely sensed continental shelf wave spectra with spectra computed by using a wave refraction model, NASA TN D-8353.

Poole, L.R., LeCroy, S.R. and Morris, W.D. 1977. Minimal-resources computer program for automatic generation of ocean wave ray or crest diagrams in shoaling waters, TM 74076.

Ross, D.B., Peloquin, R.A. Jr. and Sheil R.J. 1968. Observing ocean surface waves with a helium-neon laser, Fifth Symposium on Military Oceanography. Panama City, Florida, 18 pp.

Schule, J.J. Jr.; Simpson, L.S., and De Leonibus, P.S. 1971. A study of fetch-limited wave spectra with an airborne laser. J. Geophys. Res., 76(18):4160-4171.

St. Denis, M. and Pierson, W.J. Jr. 1953. On the motions of ships in confused seas. Trans. Soc. Naval Archit. and Mar. Eng., vol. 61, pp. 280-357.

Wilson, W.S. 1966. A method for calculating and plotting surface wave rays. U.S. Army Coastal Engineering Research Center, Tech. Memo No. 17.

APPENDIX

SYMBOLS

b	ray separation distance, meters
C	autocorrelation function
c	celerity, meters/second
d	water depth, meters
E	energy density, meters^2
F	normalized energy amplification function
f	circular frequency, hertz
g	gravitational constant, meters/second^2
H	wave height, meters
K_r	refraction coefficient
K_s	shoaling coefficient
k	wave number
ℓ	counter $(0 \leq \ell \leq M)$
L	wave length, meters
M	total number of lags
N	total number of sample data points
S	spectral density, meters^2/hertz
t	time, seconds
V	velocity, meters/second
α	angle formed by wave crest and local depth contour, degrees
η	wave elevations profile, meter
ω	radian frequency, radians/second

τ number of lags

Subscripts:

a apparent

0 initial (deepwater) value

A bar over a symbol indicates an average.

TABLE 1

GROUND TRACK OF TROPICAL STORM AMY

DATE	TIME	LATITUDE	LONGITUDE	MAX. WIND	STAGE
June 27	0000Z	27.5N	79.0W	25 KT	Trop. Dep.
	0600Z	28.5	79.0		
	1200Z	29.5	79.0		
	1800Z	30.5	79.0		
June 28	0000Z	31.5	78.8		
	0600Z	32.4	78.7		
	1200Z	33.3	78.0		
	1800Z	34.0	77.0	30	
June 29	0000Z	34.4	75.8	35	Trop. Storm
	0600Z	34.0	74.8	40	
	1200Z	33.8	73.8	45	
	1800Z	33.8	72.8	50	
June 30	0000Z	34.3	71.6		
	0600Z	35.6	70.8	55	
	1200Z	35.9	70.5	60	
	1800Z	36.2	70.2		
July 1	0000Z	36.2	69.8		
	0600Z	36.2	69.4		
	1200Z	36.2	68.3		
	1800Z	36.7	67.2		
July 2	0000Z	37.4	66.7		
	0600Z	37.3	65.9		
	1200Z	37.3	65.1		
	1800Z	37.3	64.1		
July 3	0000Z	37.7	62.8	55	
	0600Z	38.2	61.2		
	1200Z	39.3	59.6		
	1800Z	40.5	58.0	50	

TABLE 1 (Continued)

DATE	TIME	LATITUDE	LONGITUDE	MAX. WIND	STAGE
July 4	0000Z	42.5	54.8		
	0600Z	44.5	51.6		
	1200Z	47.0	48.0	45	Extra-Tropical

TABLE 2

FLIGHT NAVIGATION LOG

TIME (EDT)			LATITUDE		LONGITUDE	
Hr.	Min.	Sec.	Degrees	Minutes	Degrees	Minutes
16	12	00	36	33.9N	74	15.4W
16	14	00	-	-	-	-
16	16	00	36	28.8	74	27.2
16	18	00	36	26.3	74	32.7
16	20	00	36	23.3	74	38.7
16	22	00	36	20.4	74	44.6
16	24	00	36	17.3	74	51.1
16	26	00	36	14.8	74	56.5
16	28	00	36	11.3	75	04.1
16	30	00	36	09.3	75	08.0
16	32	00	36	06.4	75	13.7
16	34	00	36	03.5	75	14.7
16	36	00	36	00.9	75	25.0
16	39	26	35	55.1	75	34.1

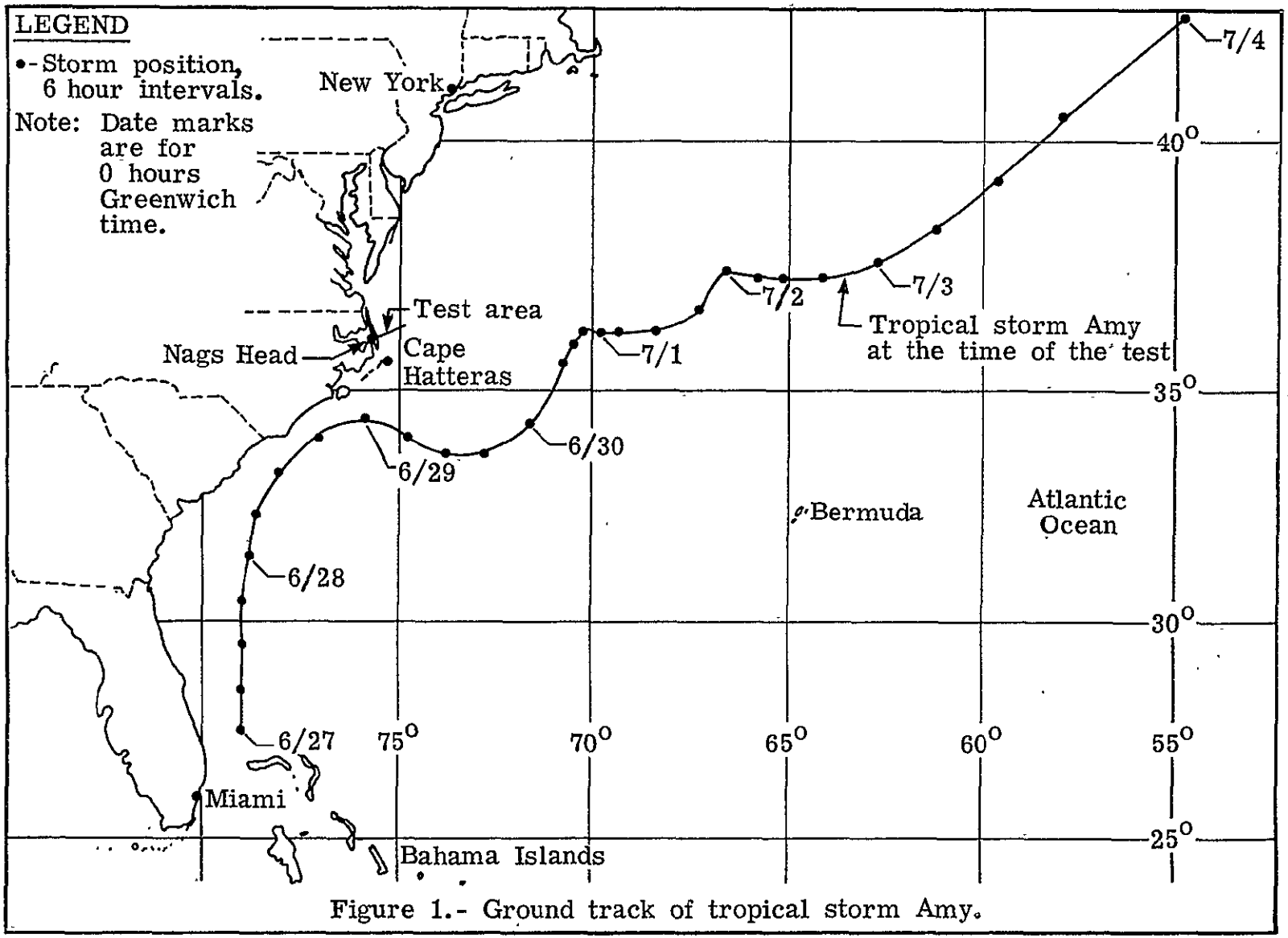

Figure 1.- Ground track of tropical storm Amy.

Figure 2.- Photograph of tropical storm Amy, 1500 GMT, July 2, 1975, taken from the Synchronous Meterological Satellite-1.

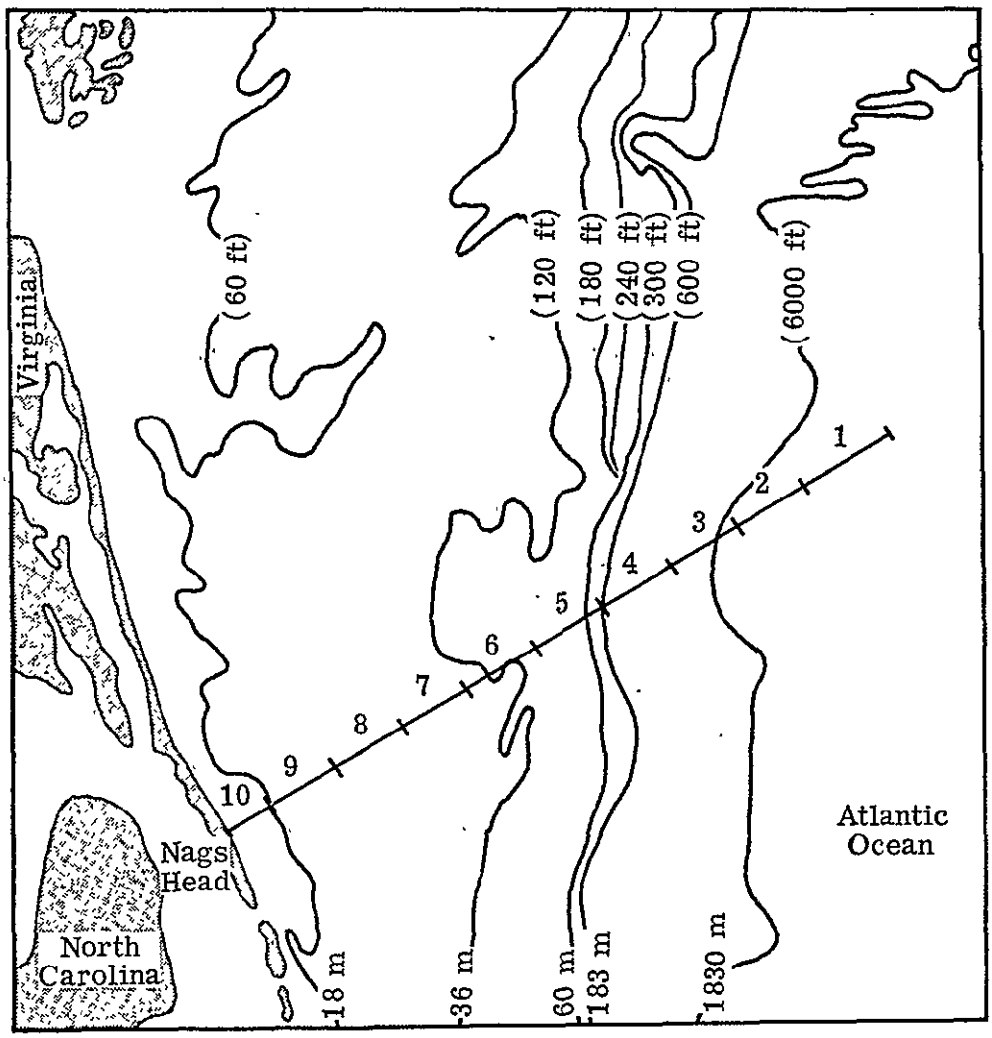

Figure 3.- Numbered spectral segments along the flight line. Contour depths in meters (feet).

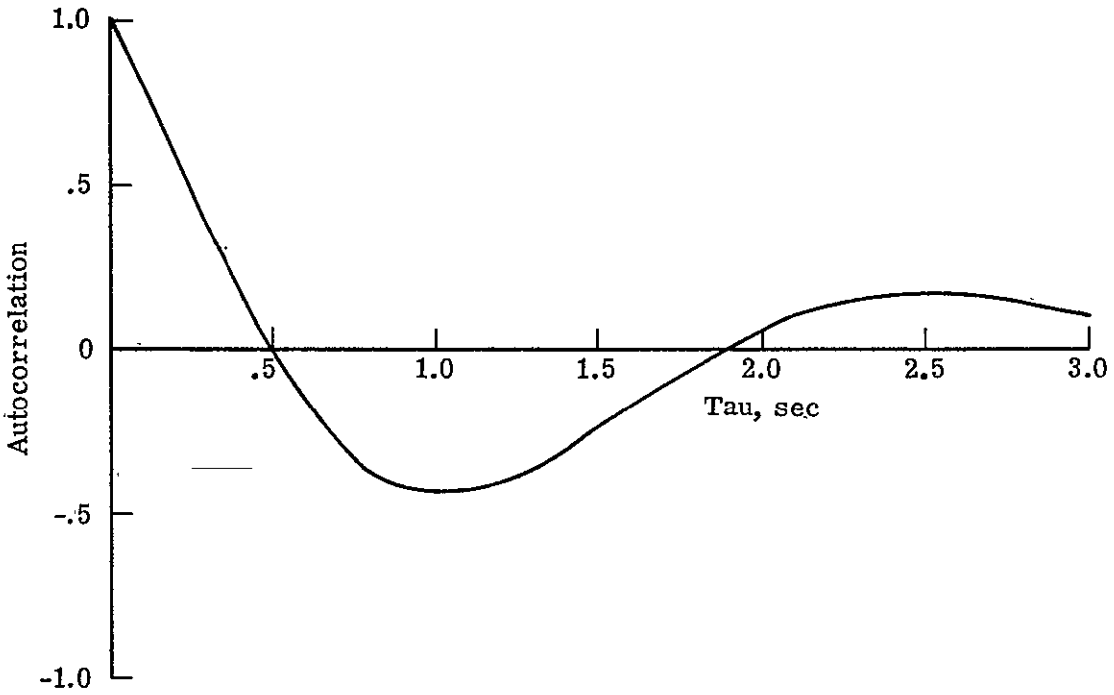

Figure 4.- Autocorrelation for surface elevation as a function of lag time.

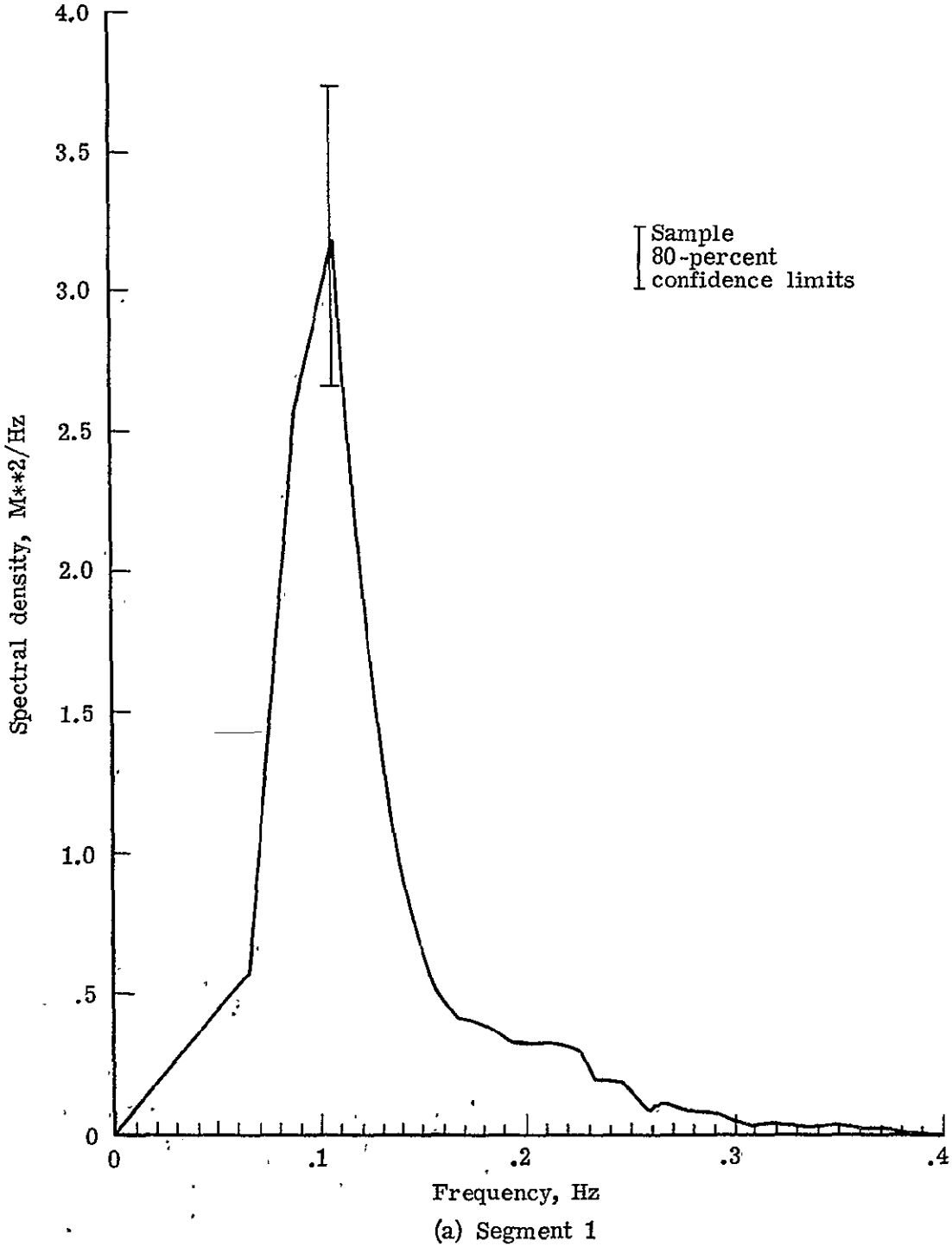

(a) Segment 1

Figure 5.- Experimental deep-water spectra for flight track segments.

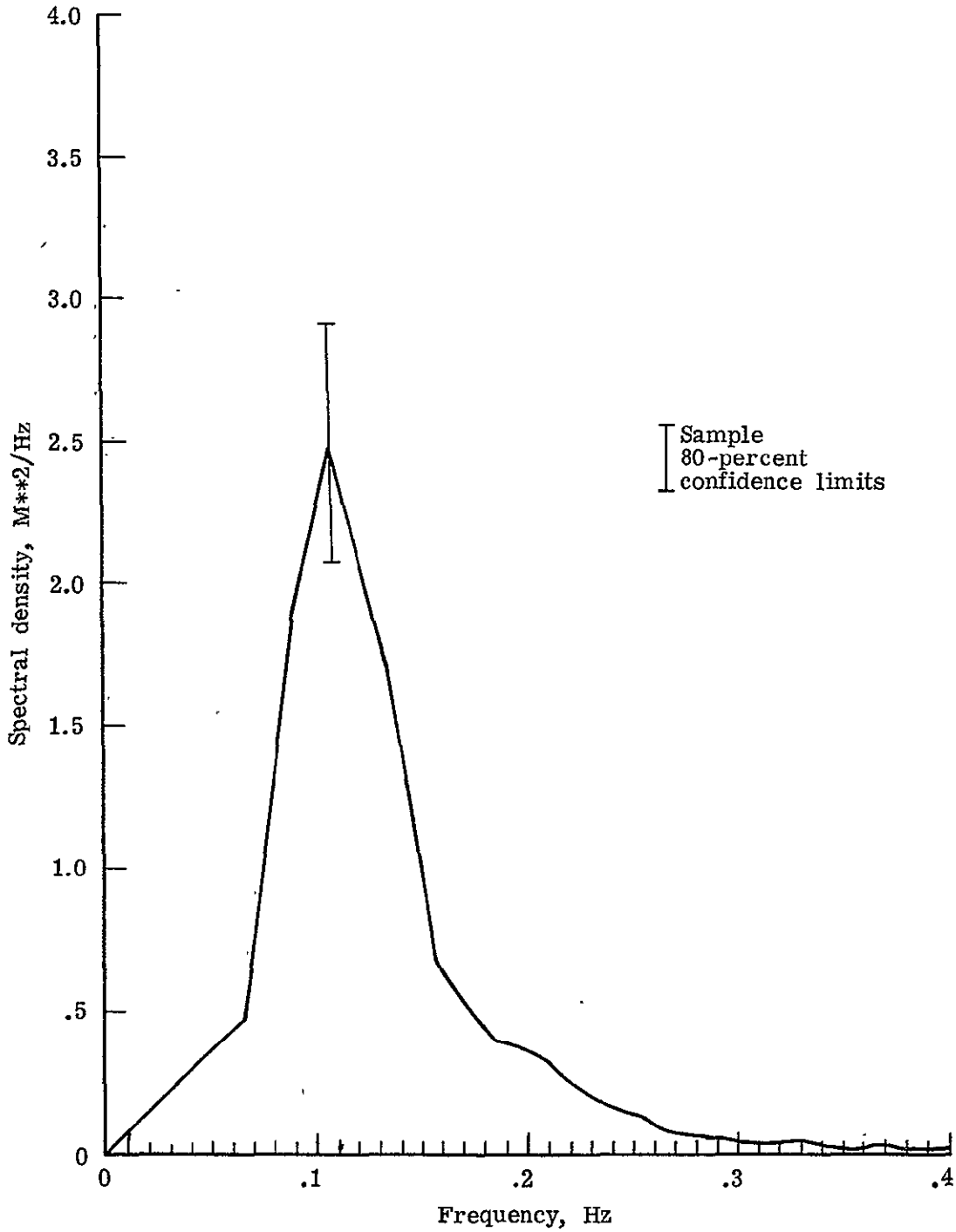

(b) Segment 2

Figure 5.- Continued

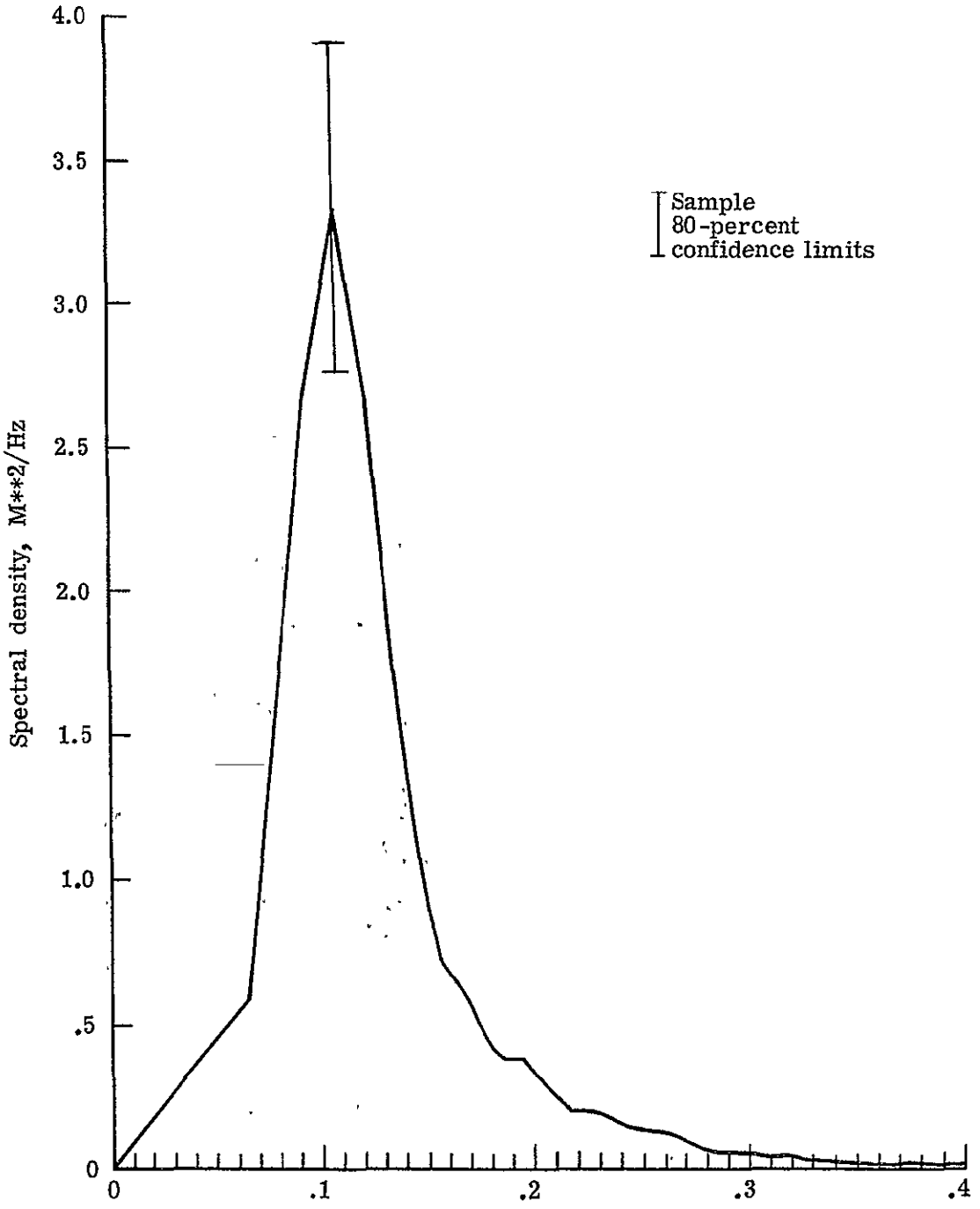

(c) Segment 3

Figure 5.- Continued

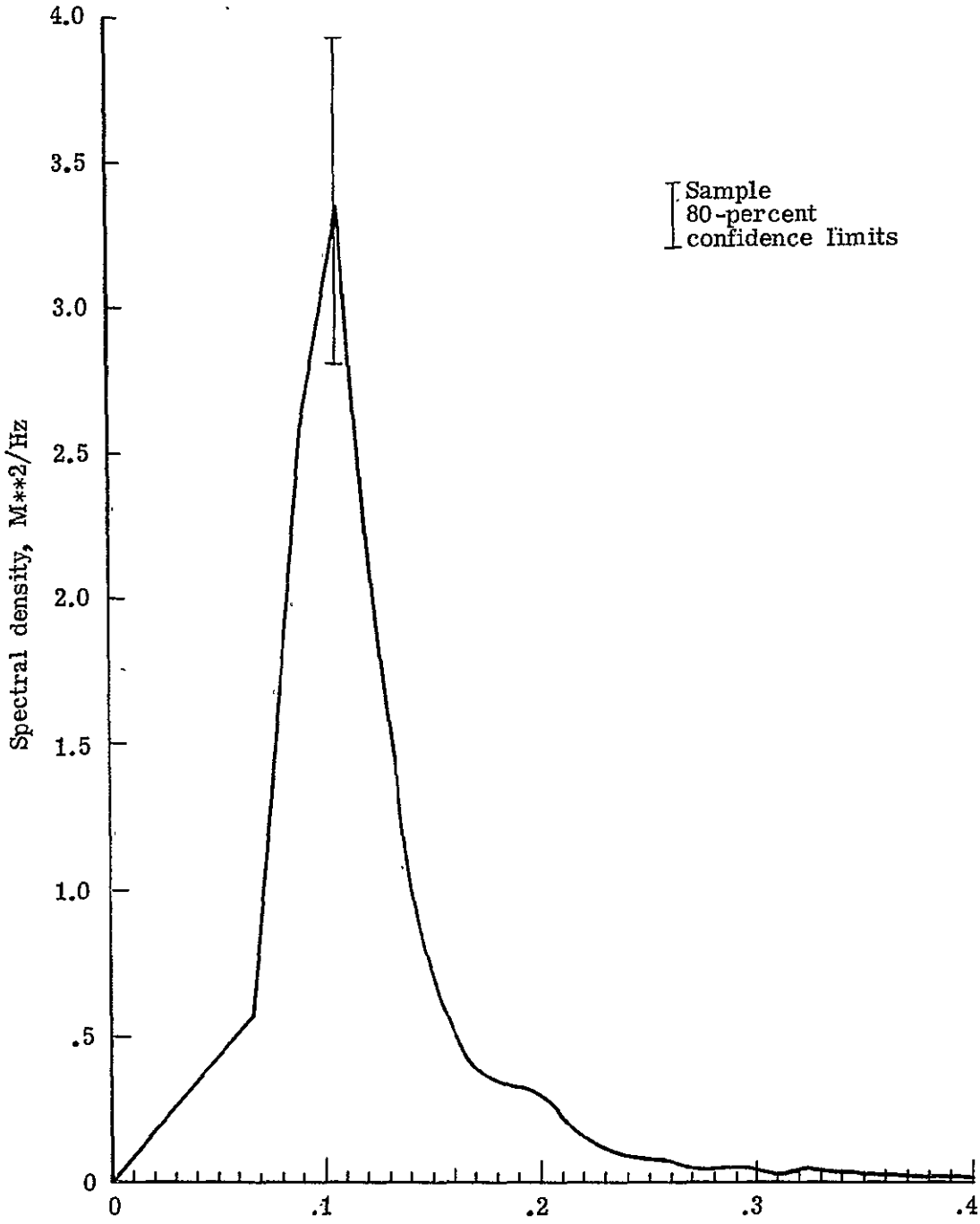

(d) Segment 4

Figure 5.- Concluded

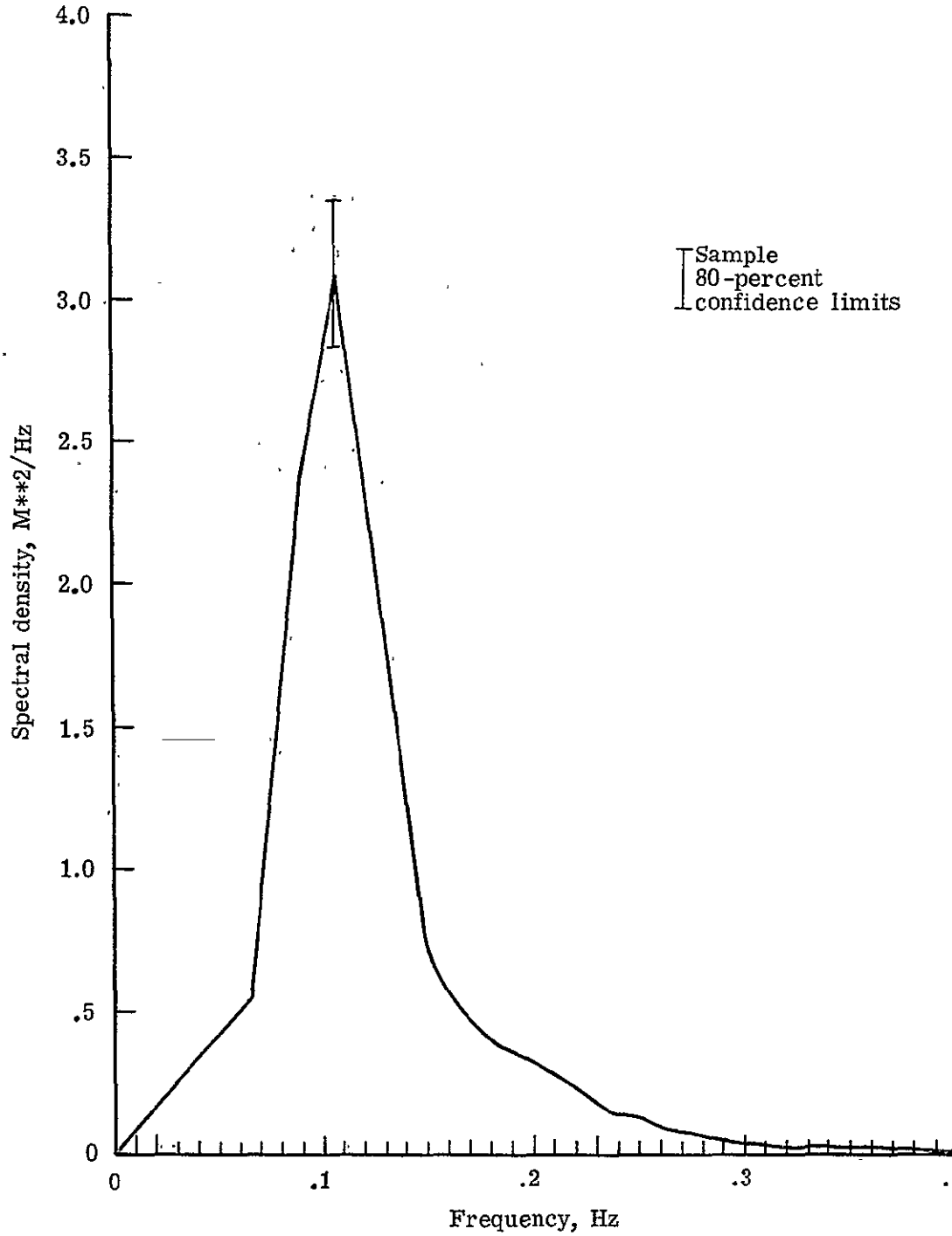

Figure 6.- Deep-water reference spectrum.

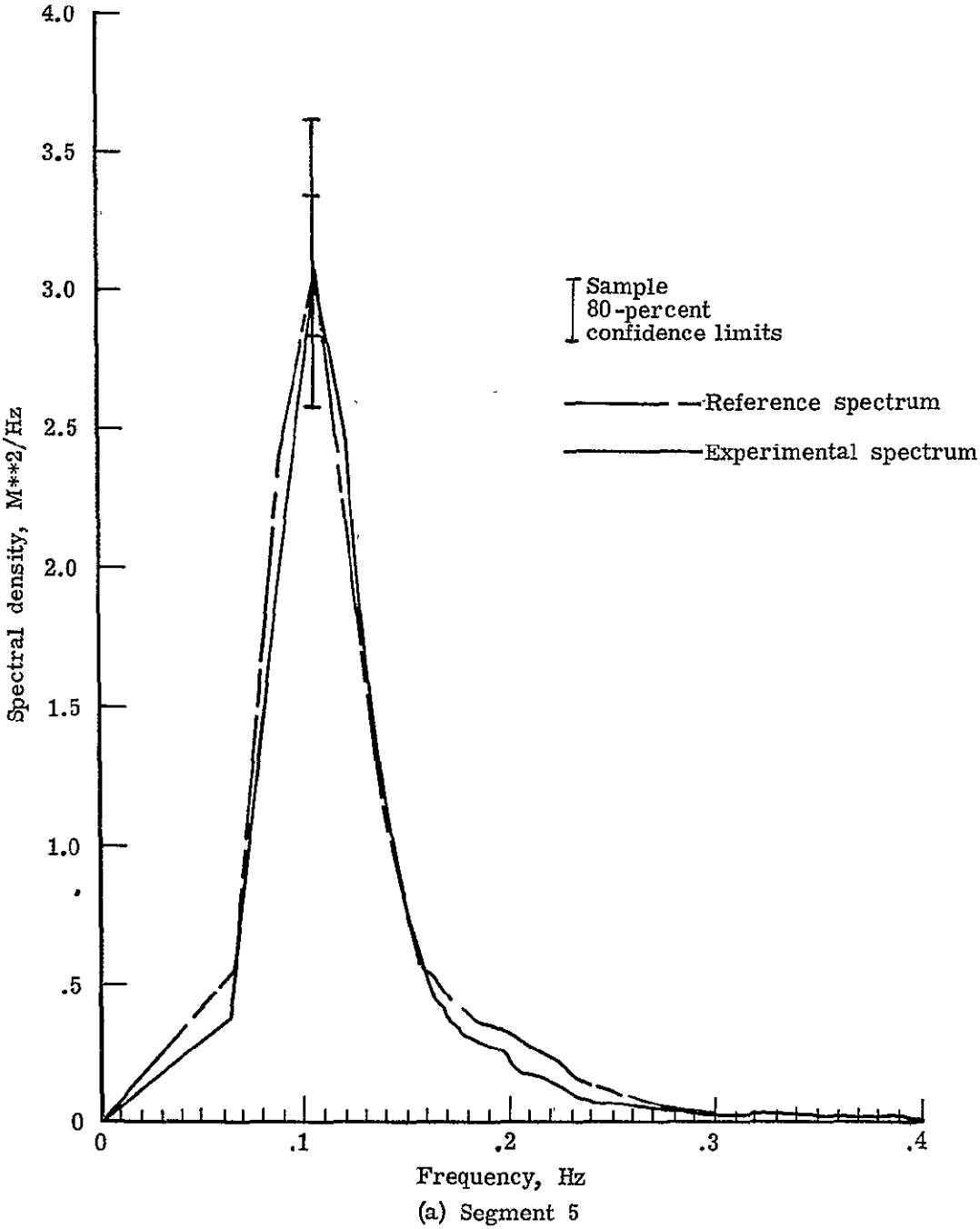

(a) Segment 5

Figure 7.- Comparison of the experimental spectra with the reference spectra for each data segment.

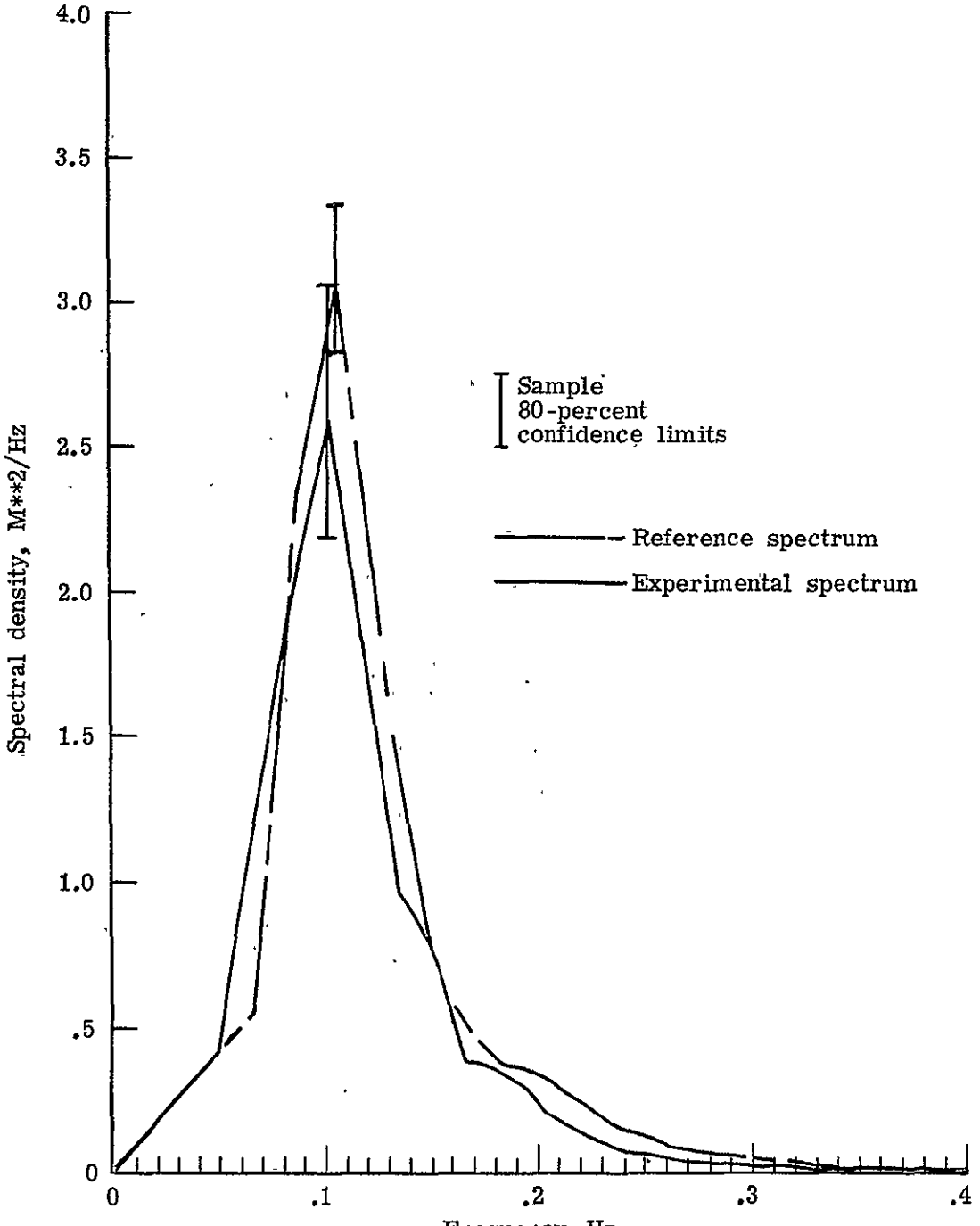

(b) Segment 6

Figure 7.- Continued

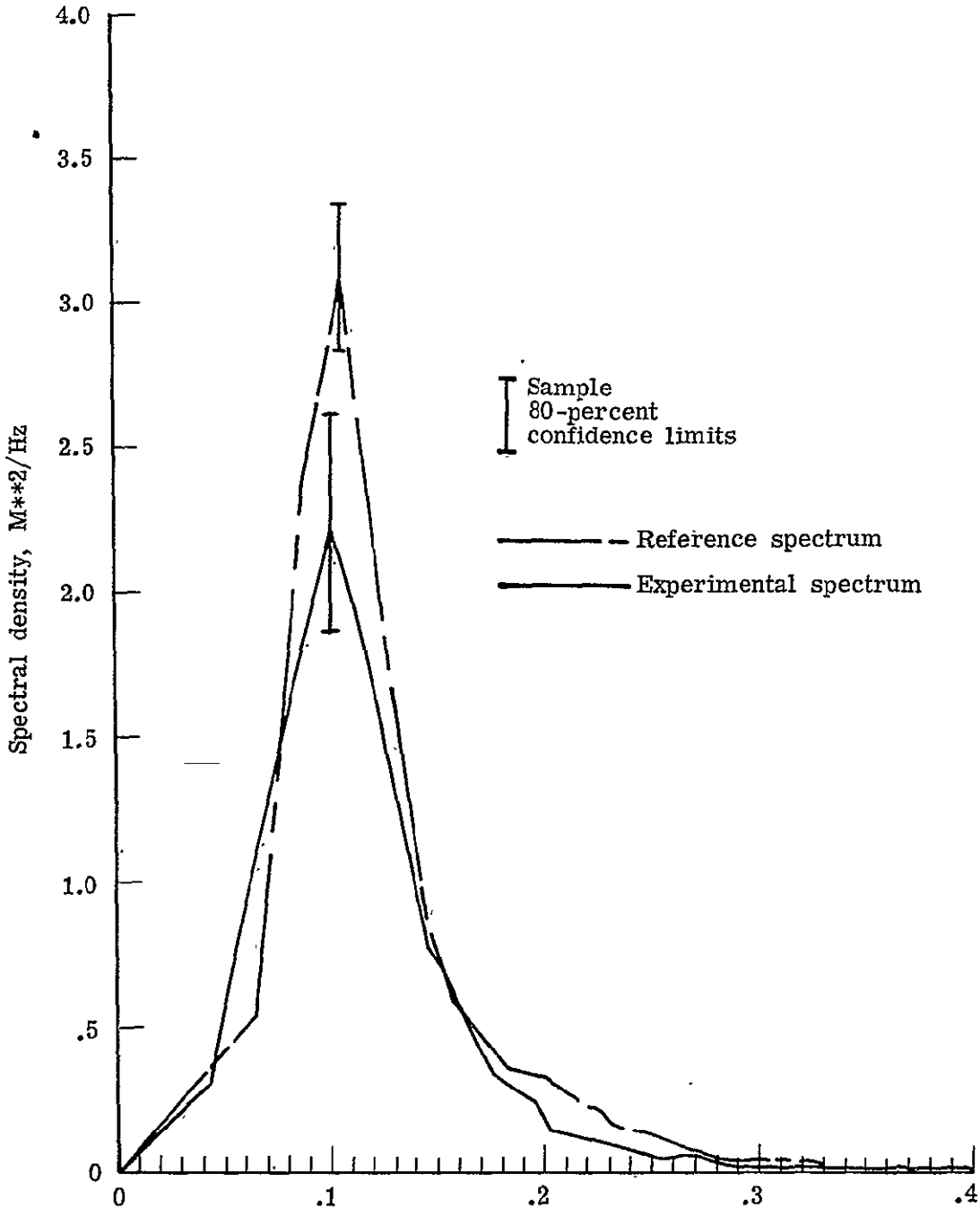

(c) Segment 7

Figure 7.- Continued

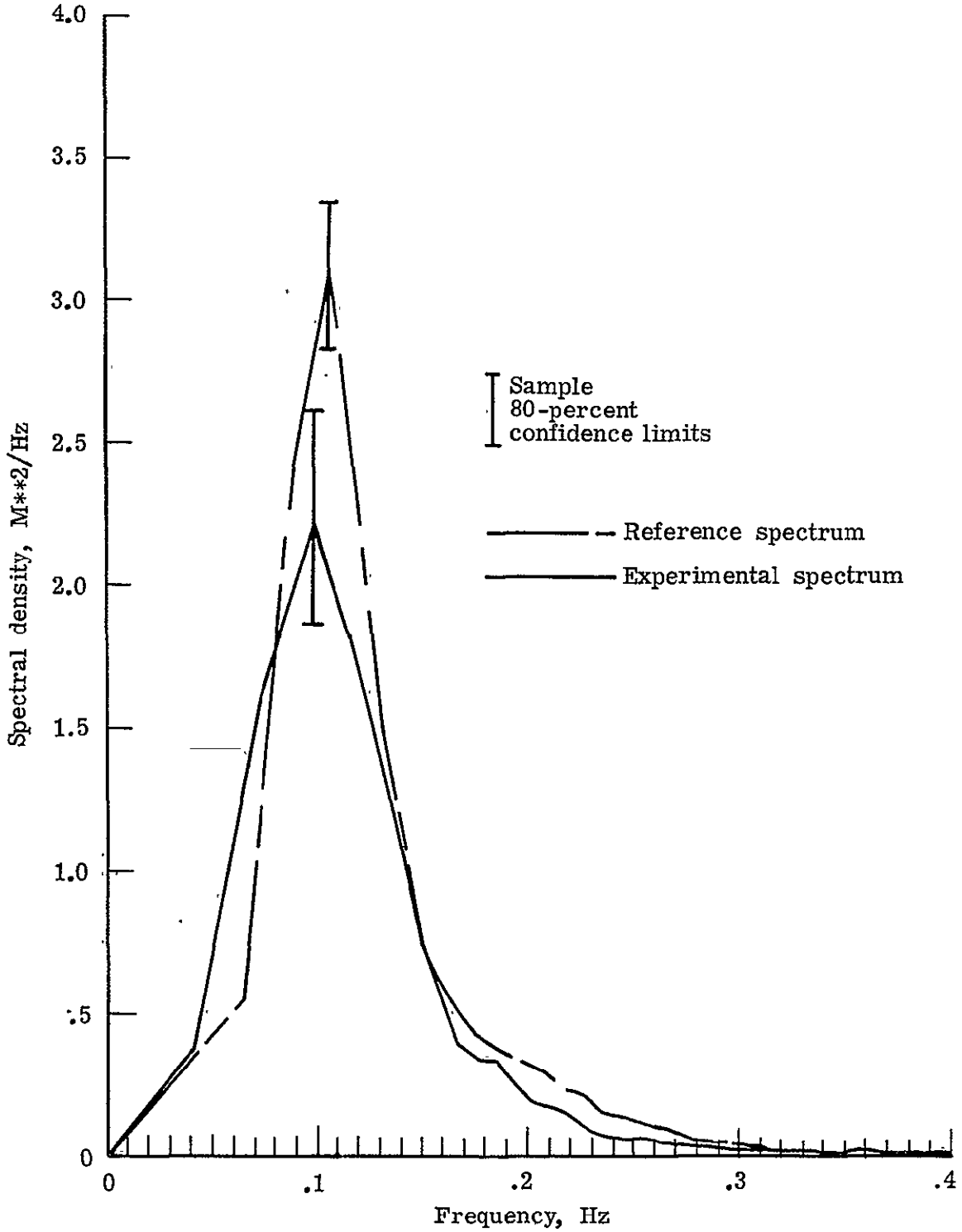

(d) Segment 8

Figure 7.- Continued

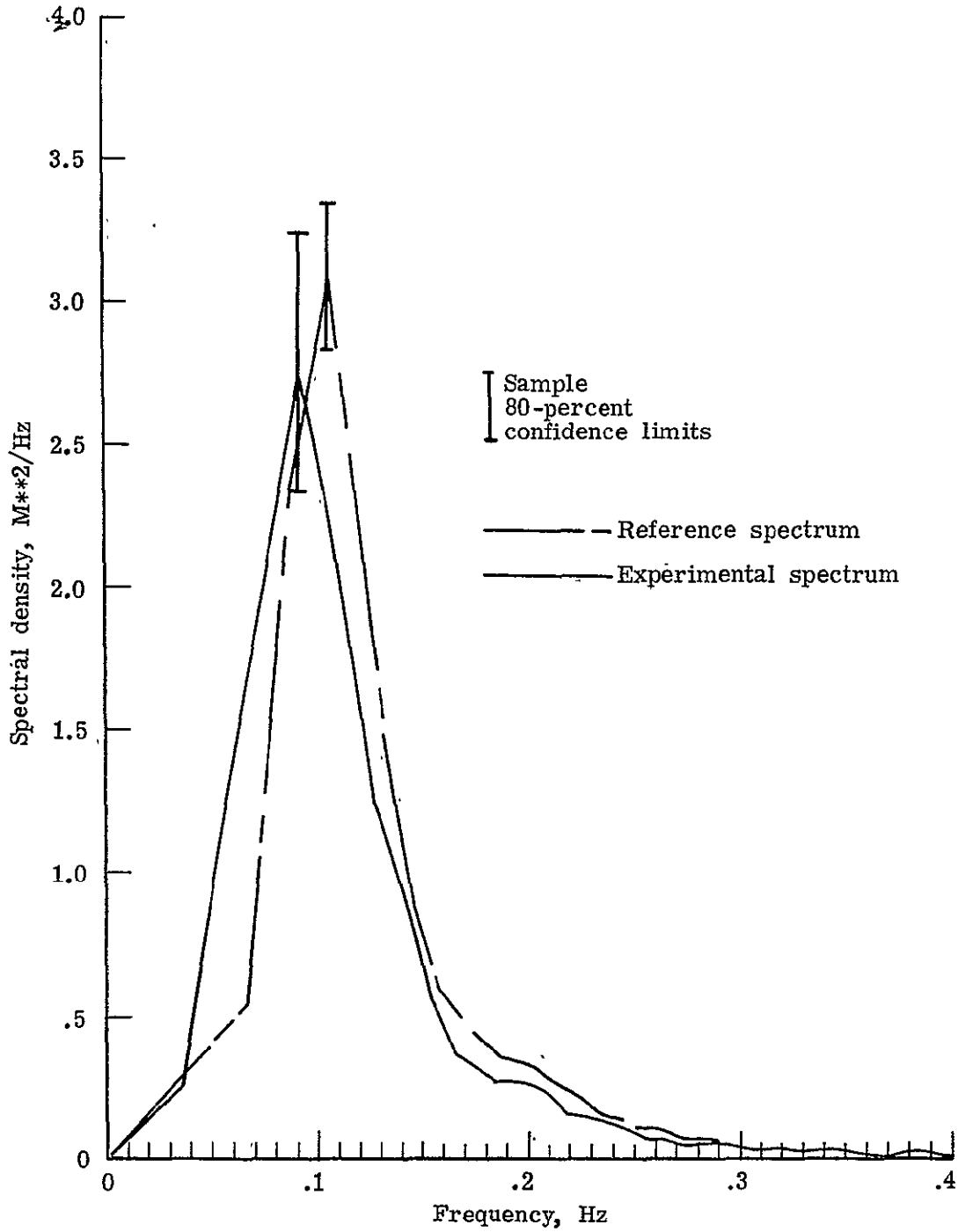

(e) Segment 9

Figure 7.- Continued

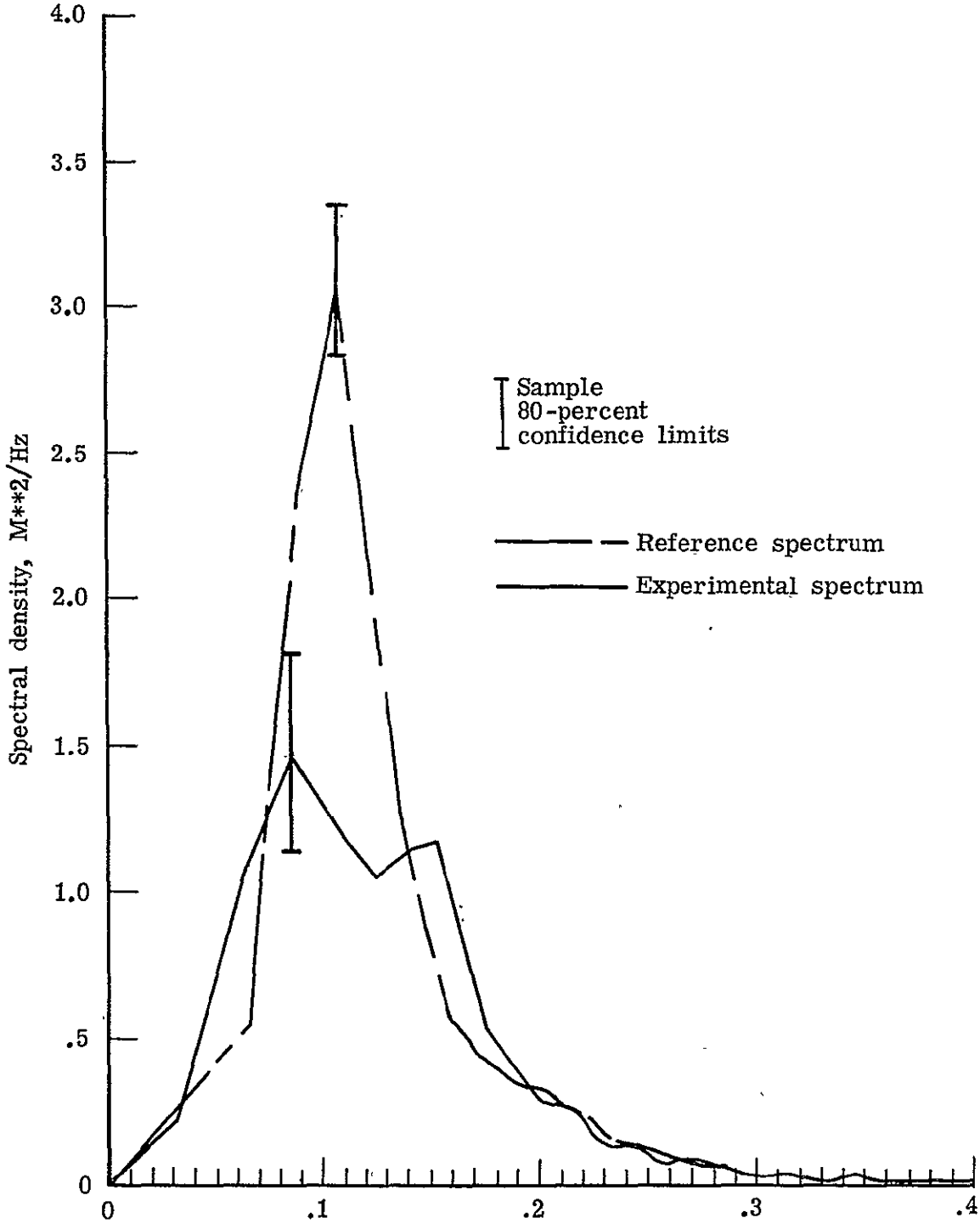

(f) Segment 10

Figure 7.- Concluded

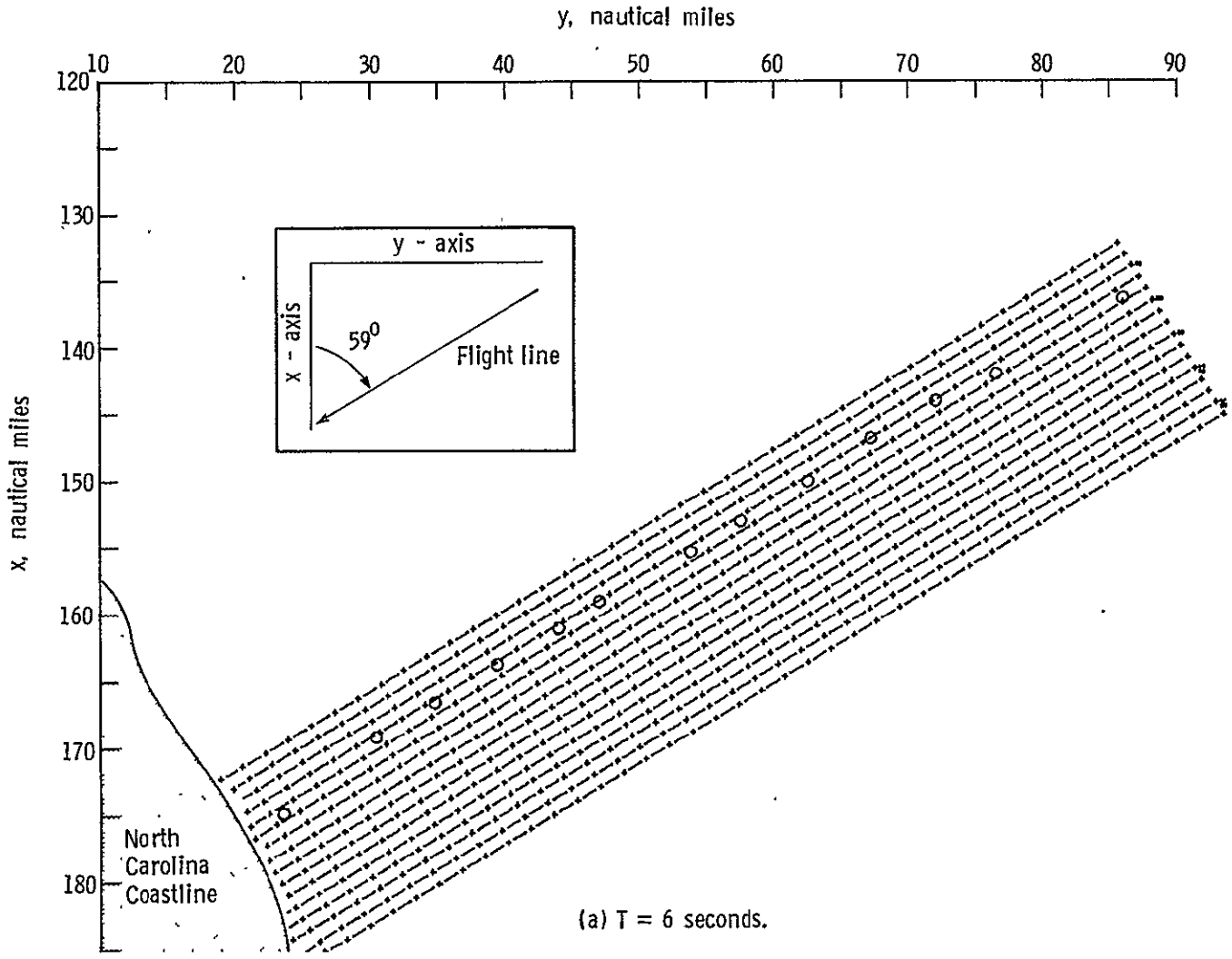

Figure 8.- Refraction diagrams for typical wave periods of the wave field. Wave crest locations at equal time intervals are marked by an x. Circular symbols denote inertial navigation points.

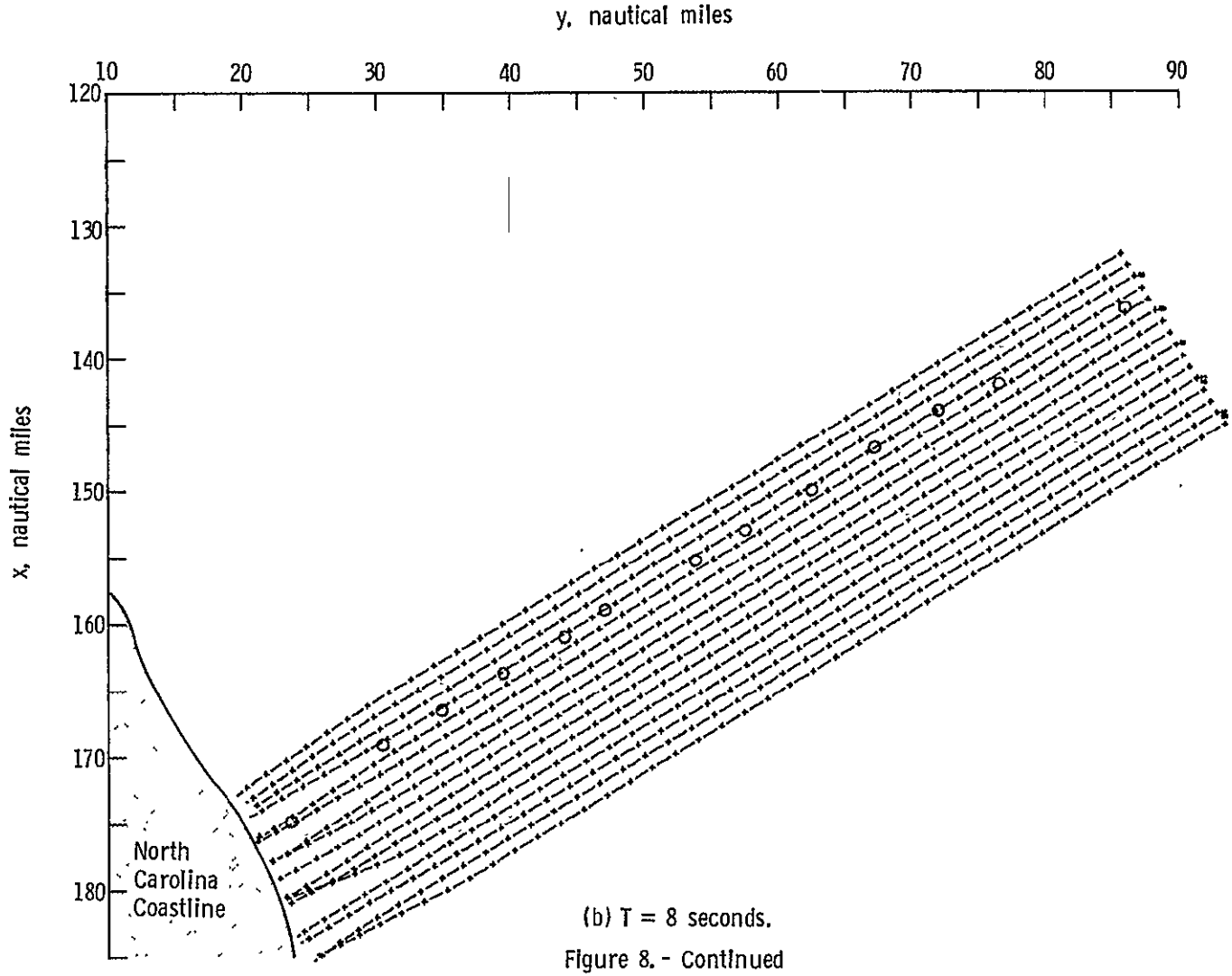

(b) T = 8 seconds.

Figure 8. - Continued

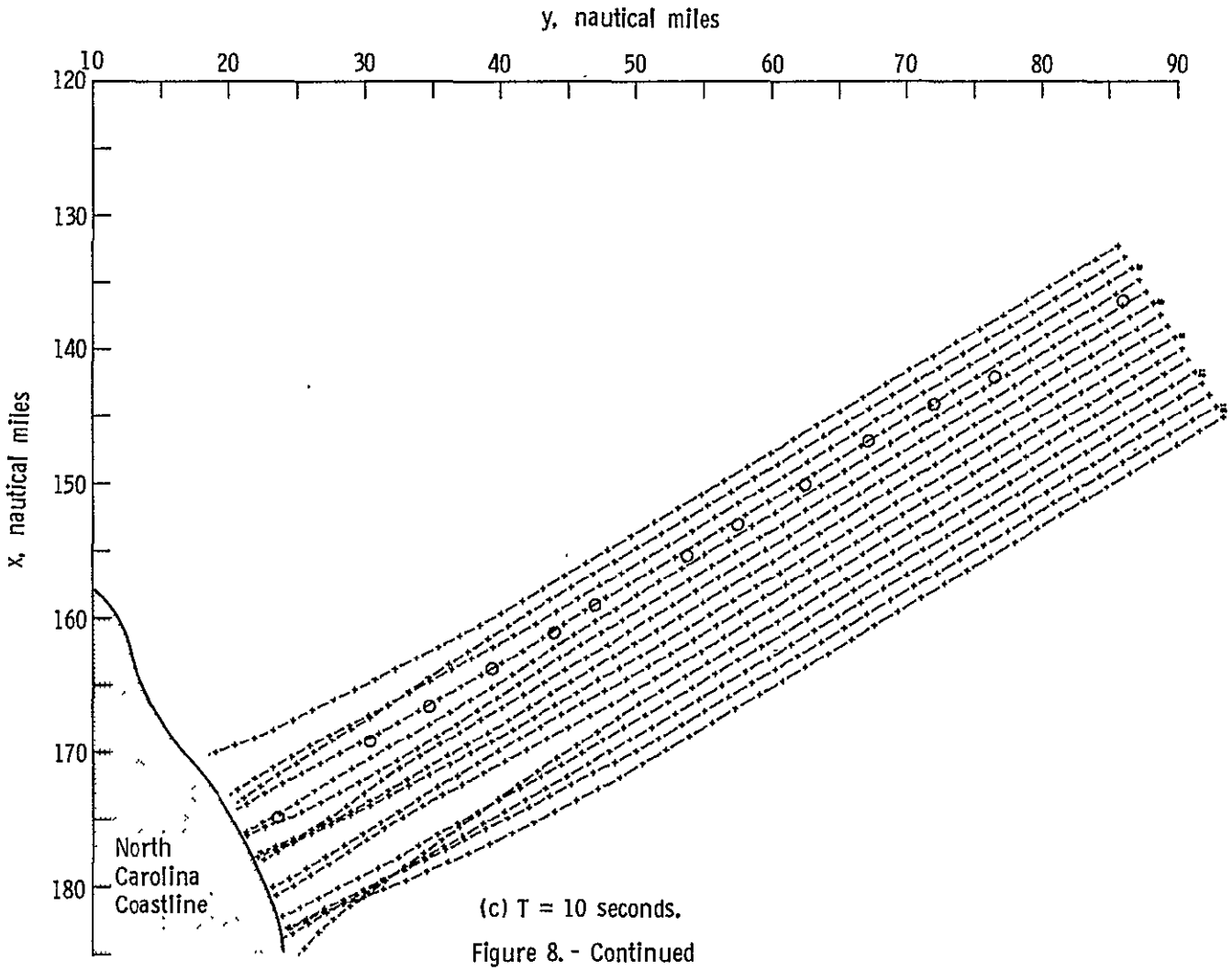

(c) T = 10 seconds.

Figure 8. - Continued

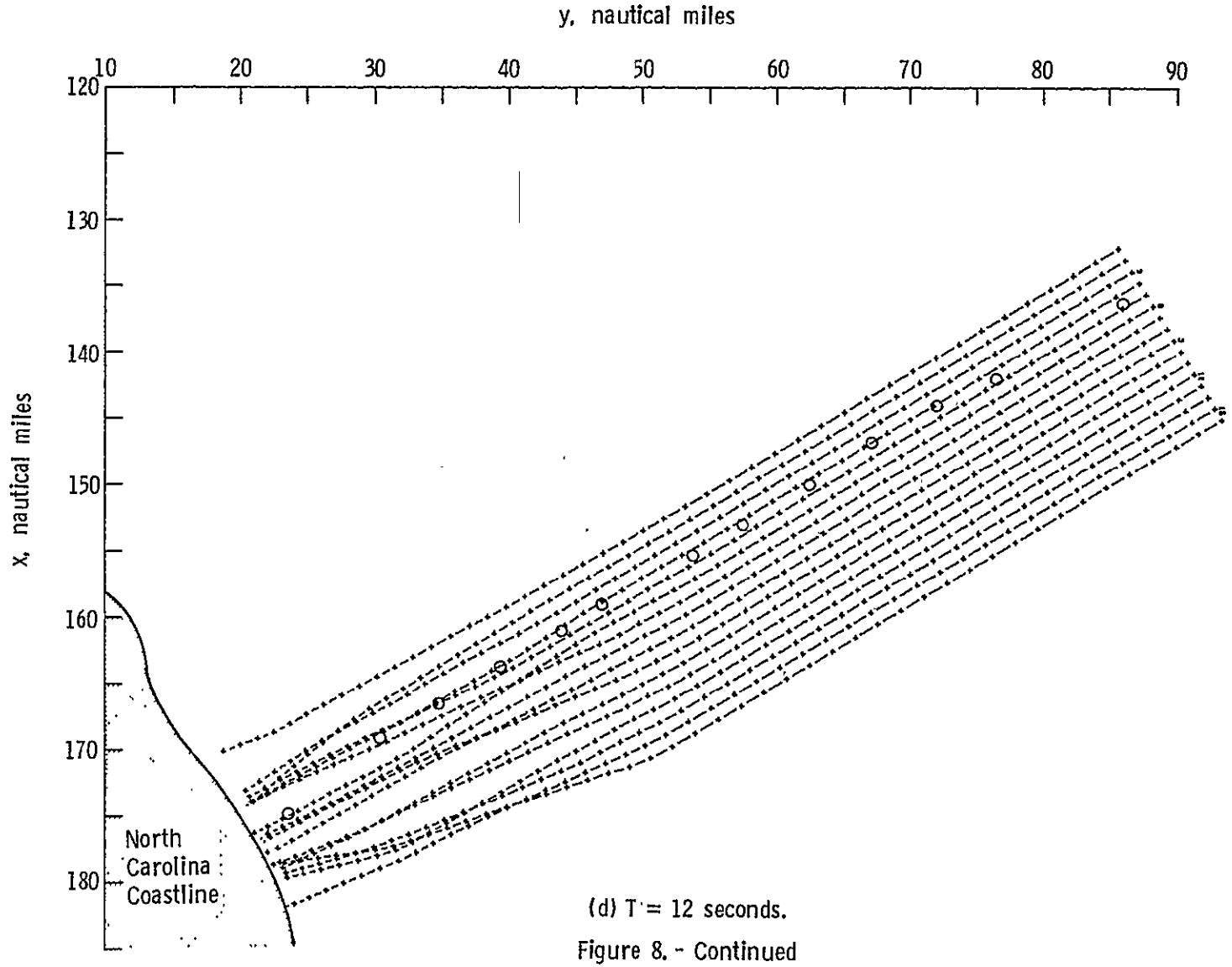

(d) T = 12 seconds.

Figure 8. - Continued

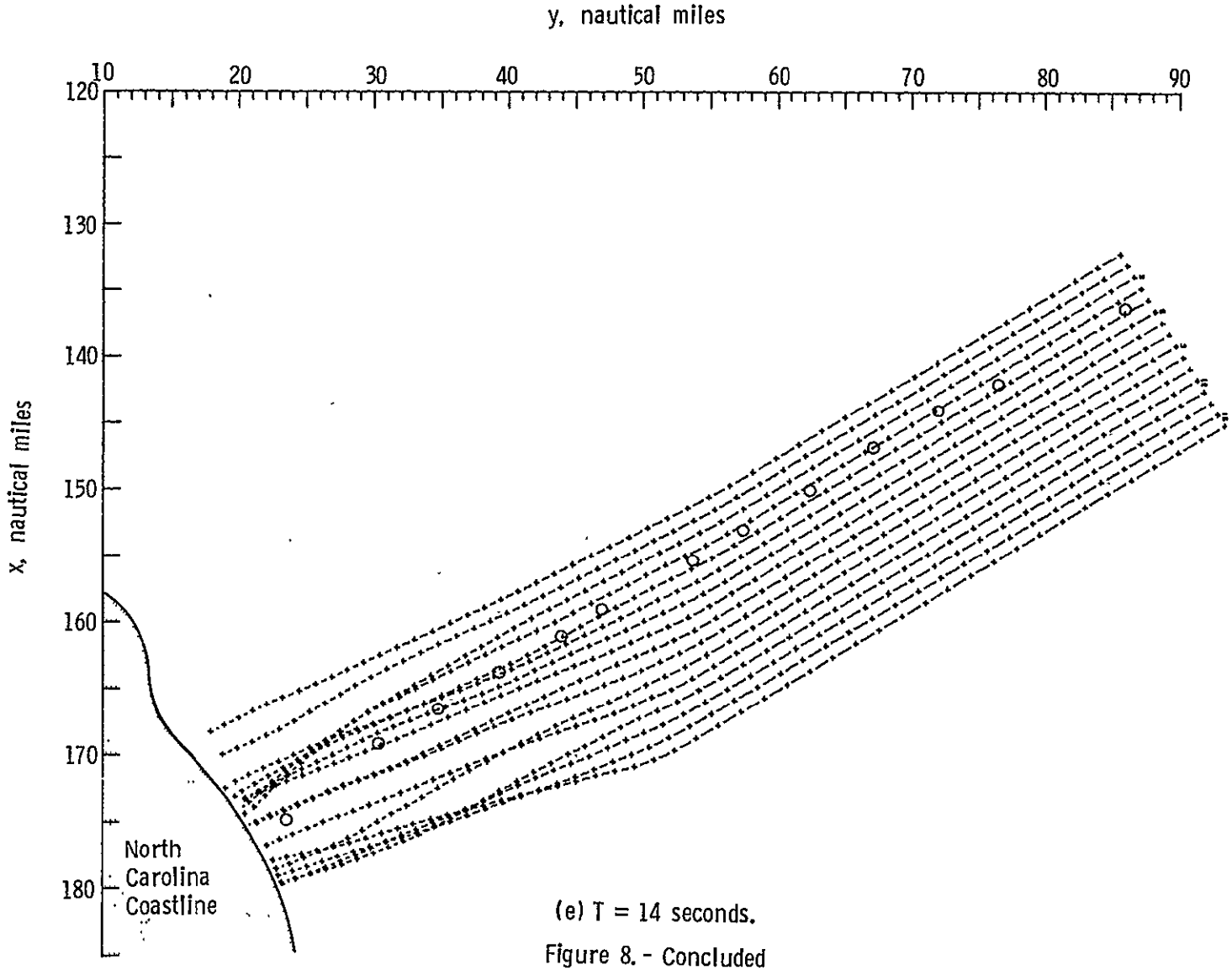

(e) T = 14 seconds.

Figure 8. - Concluded

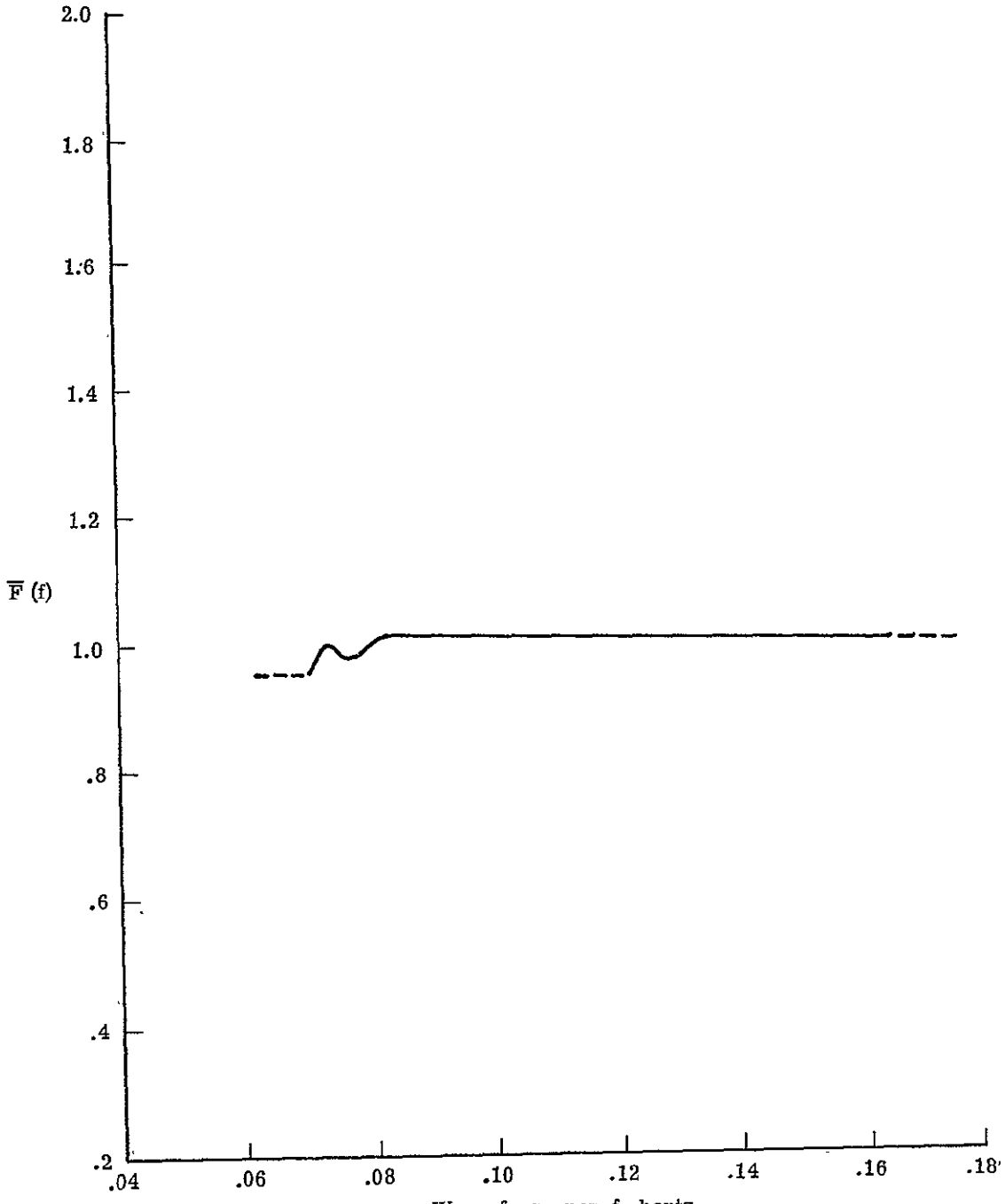

(a) Segment 5

Figure 9.- Spatially averaged energy amplification functions for flight track segments. Dashed line indicates assumed values.

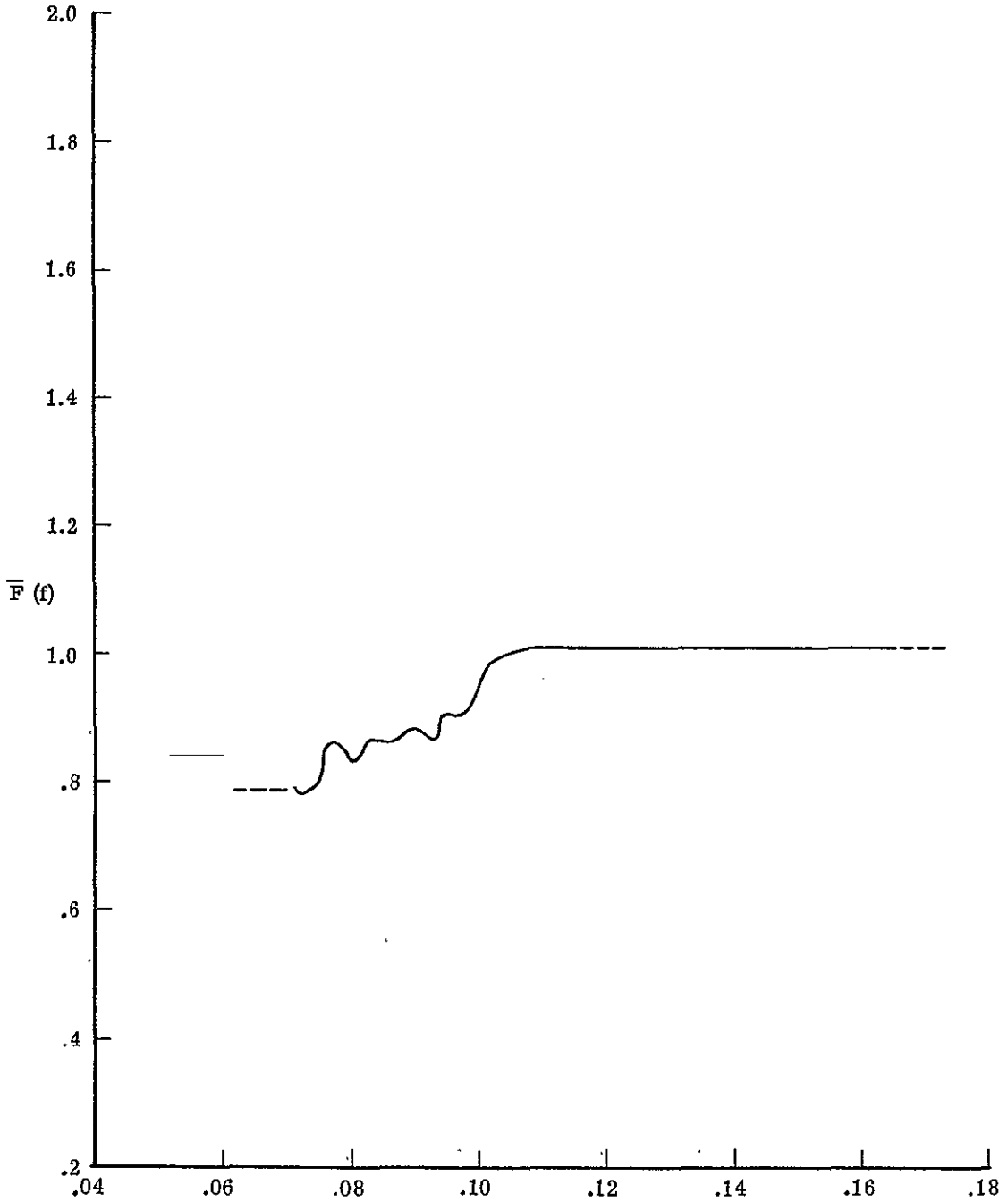

(b) Segment 6

Figure 9.- Continued

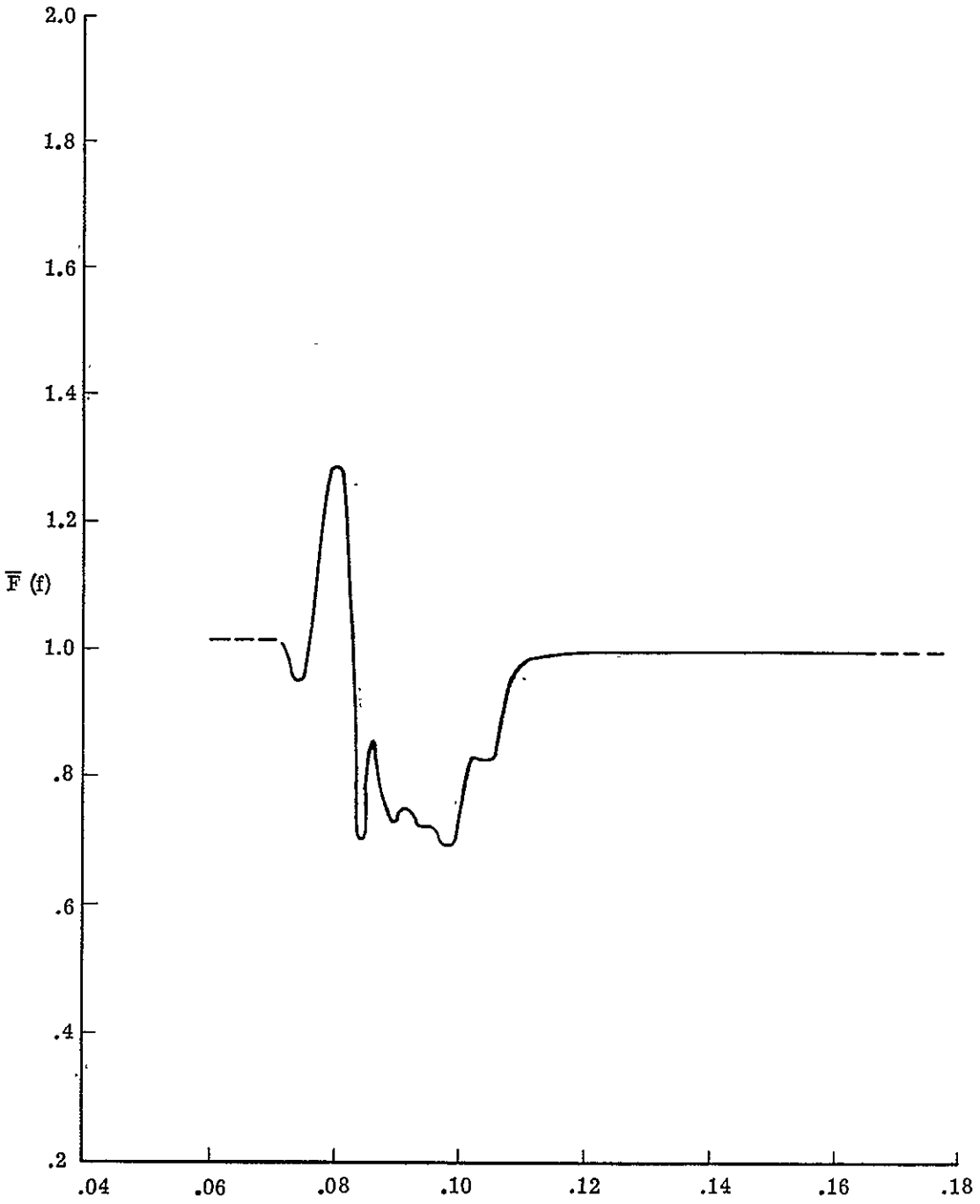

(c) Segment 7

Figure 9.- Continued

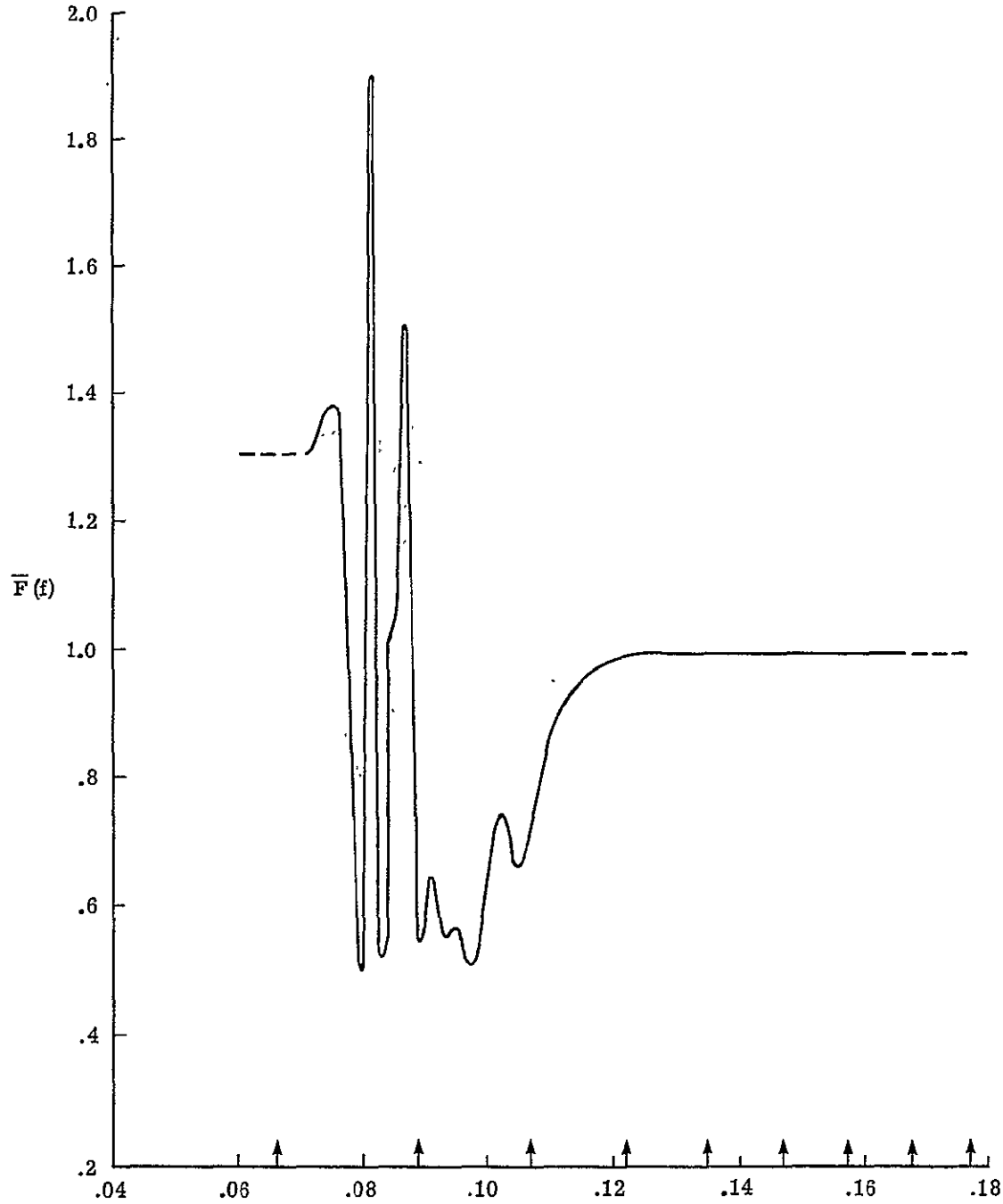

(d) Segment 8

Figure 9.- Continued

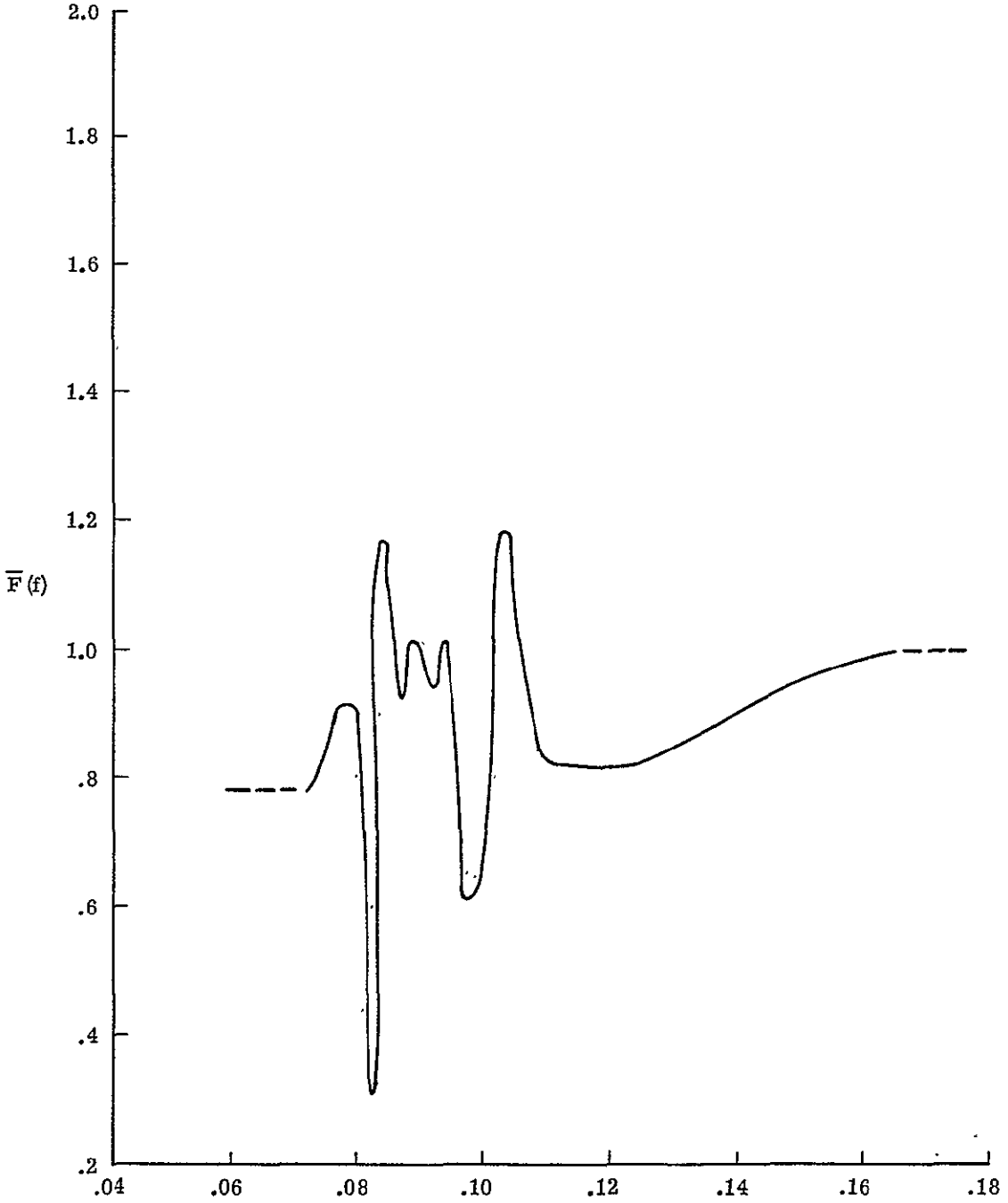

(e) Segment 9

Figure 9.- Continued

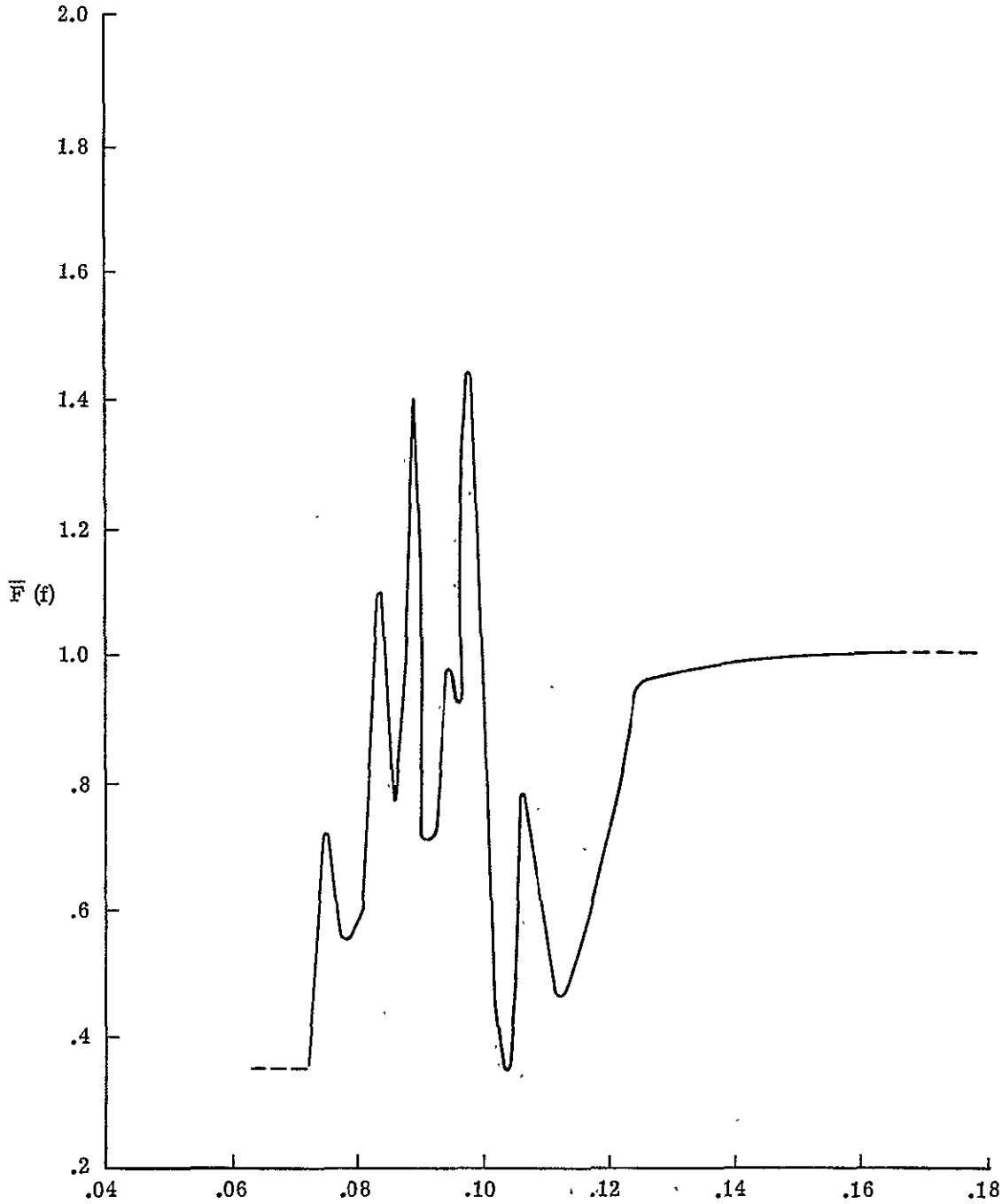

(f) Segment 10

Figure 9.- Concluded

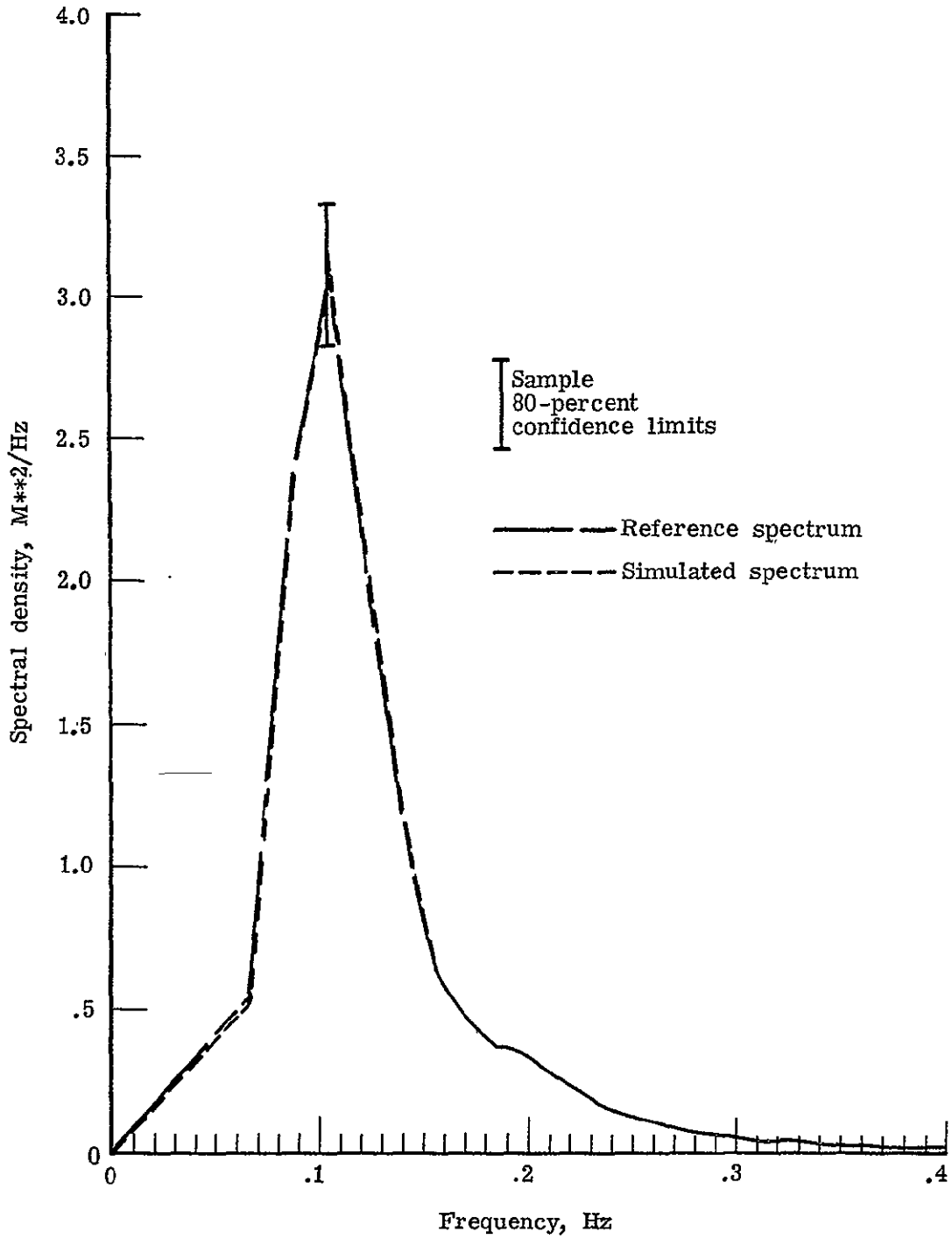

(a) Segment 5

Figure 10.- Comparison of the simulated spectra with the reference spectra for each data segment.

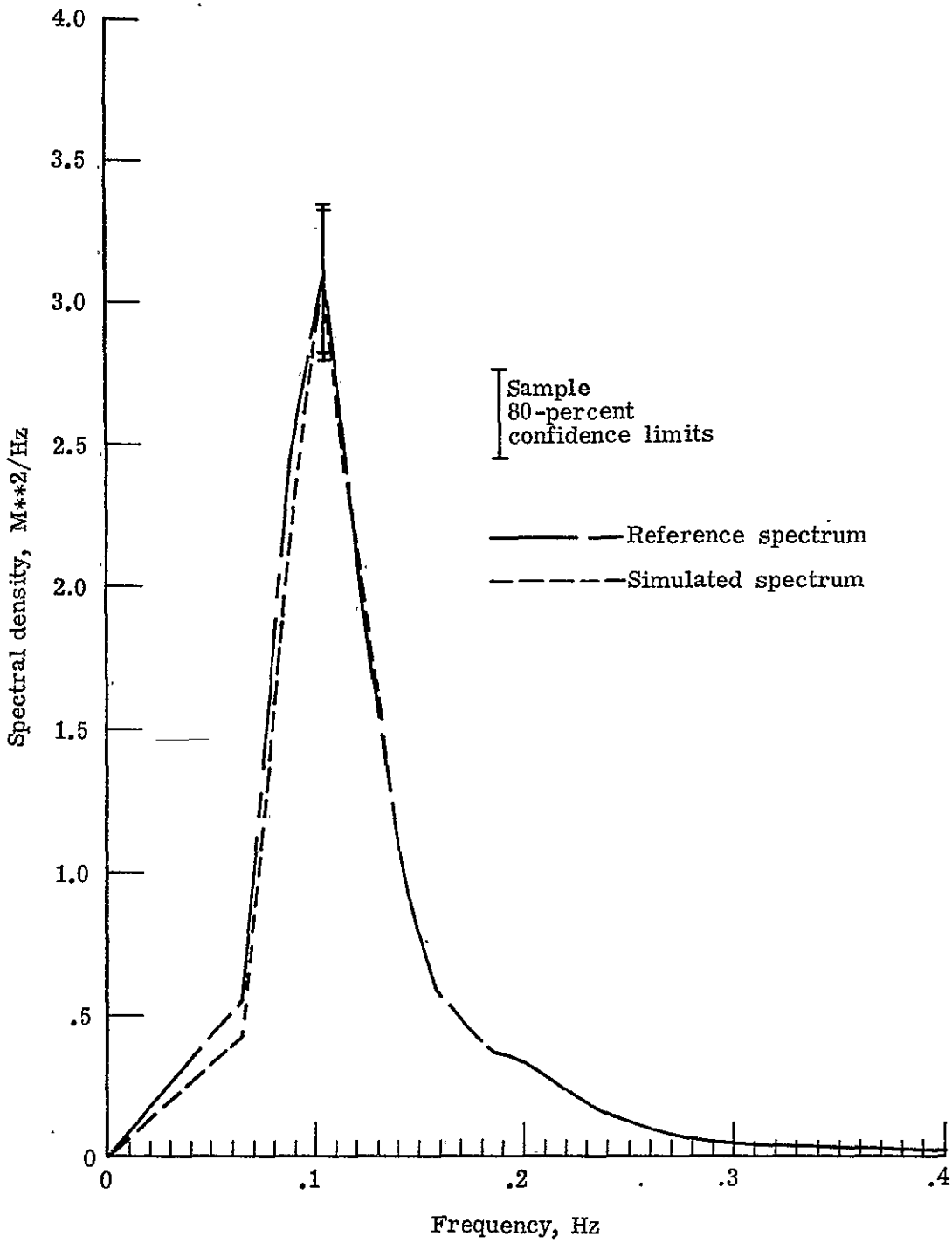

(b) Segment 6

Figure 10.- Continued

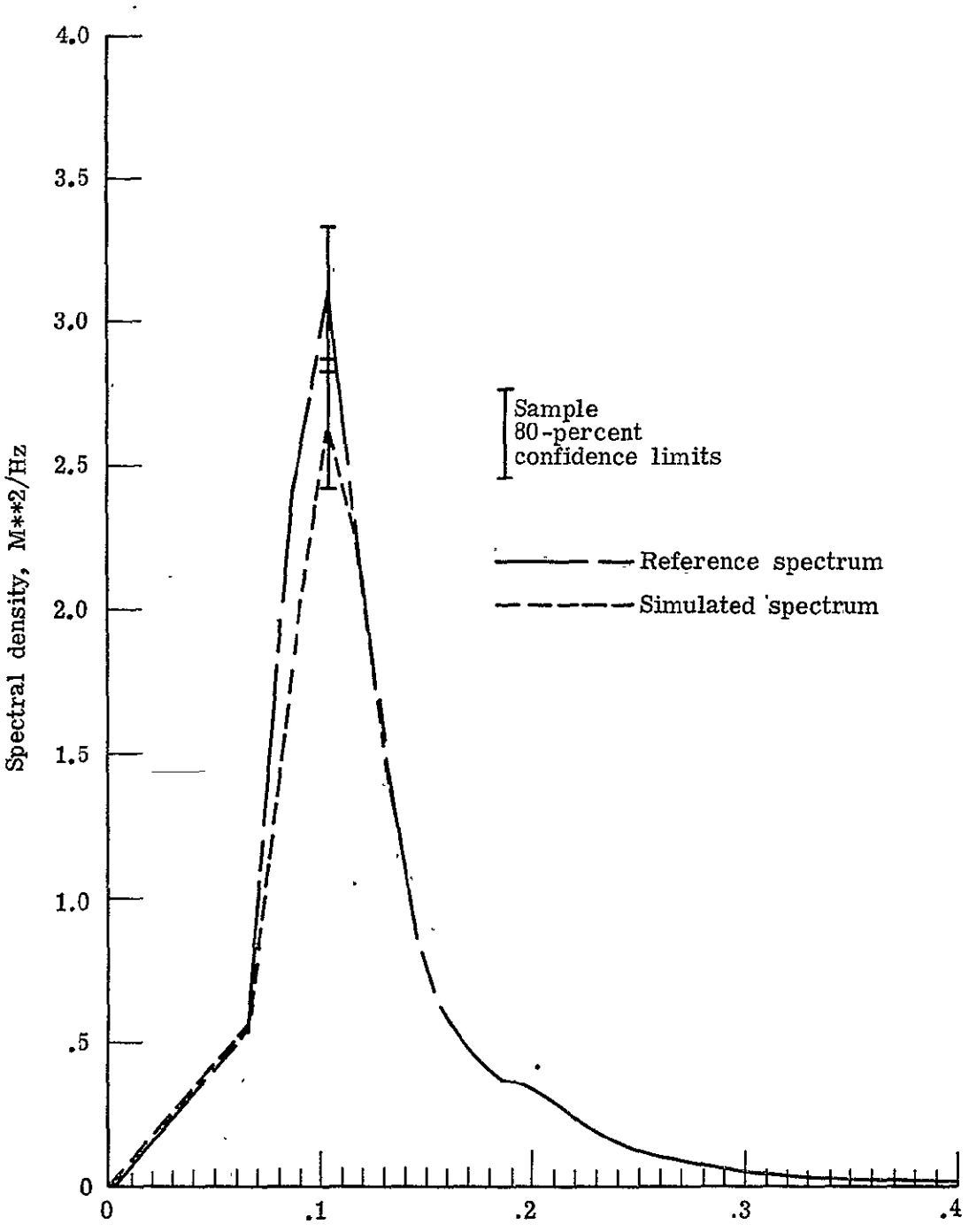

(c) Segment 7

Figure 10.- Continued

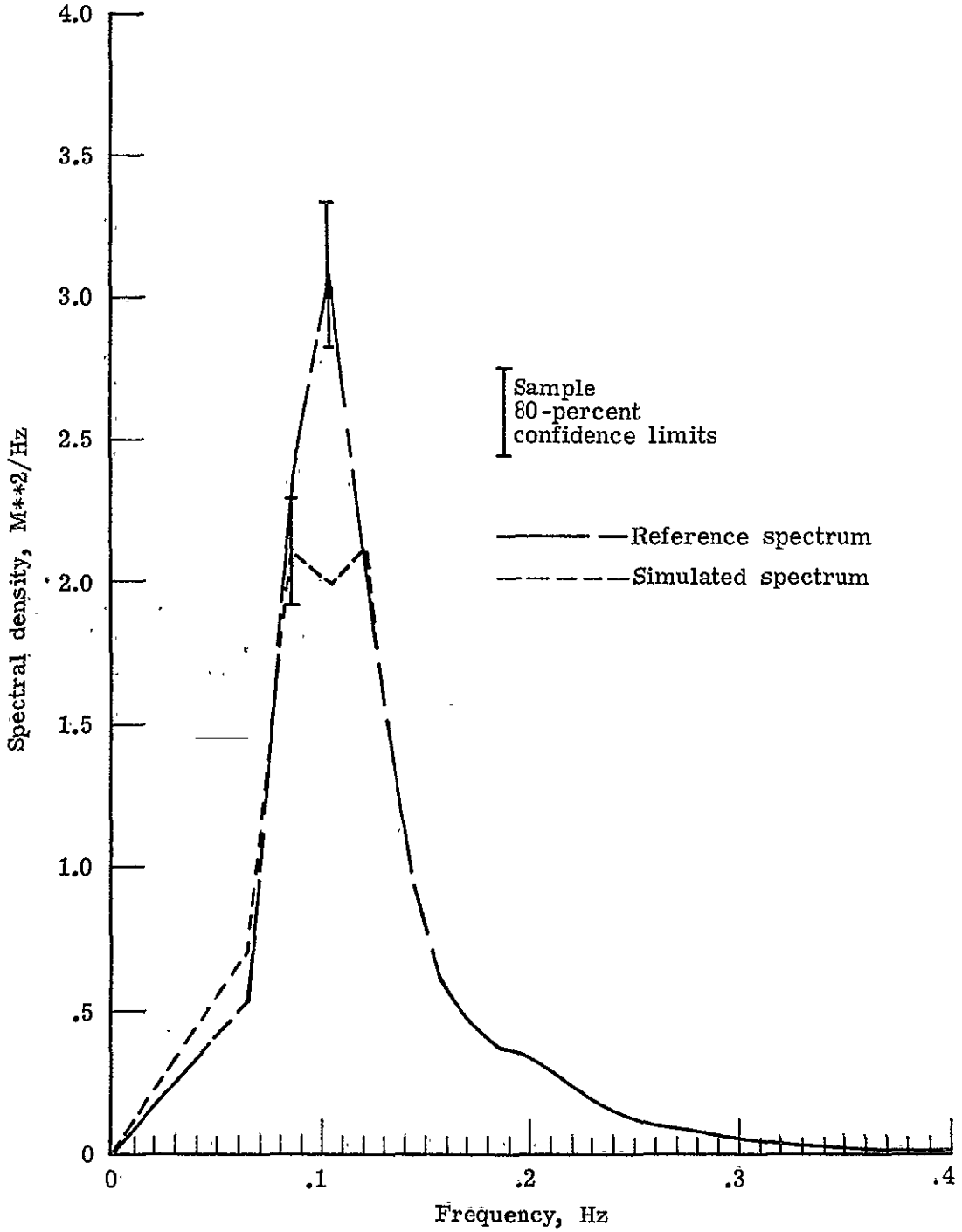

(d) Segment 8.

Figure 10.- Continued

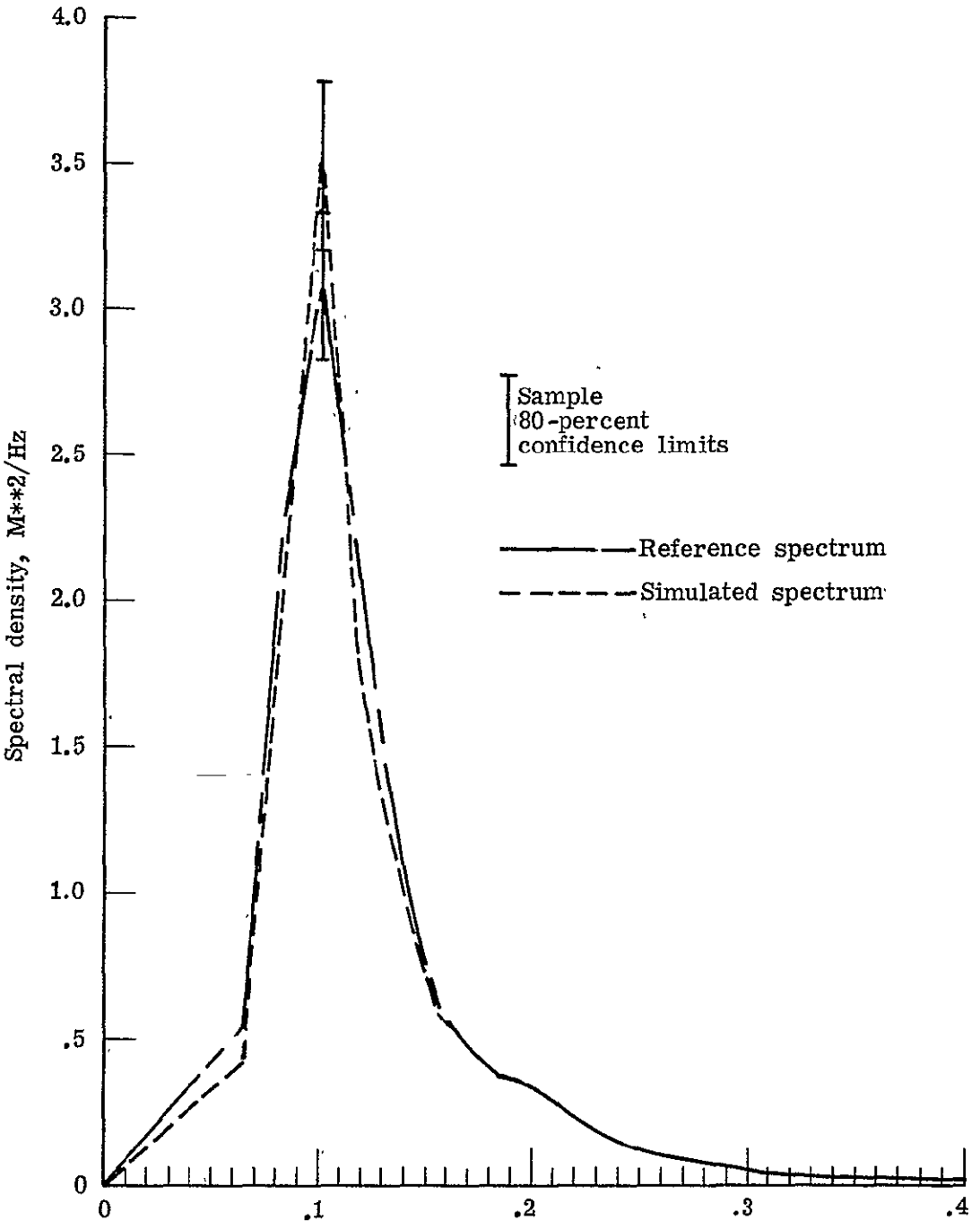

(e) Segment 9

Figure 10.- Continued

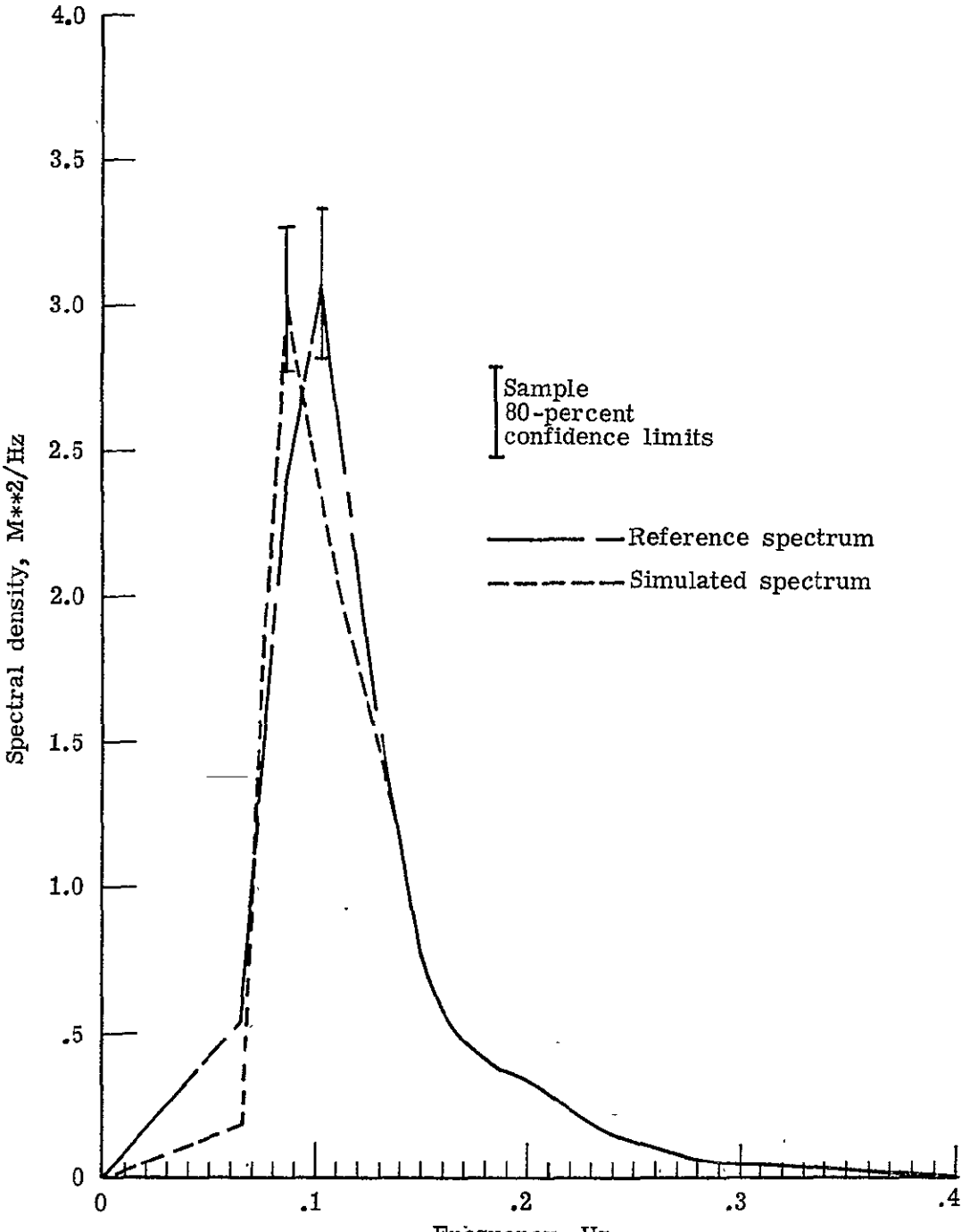

(f) Segment 10

Figure 10.- Concluded

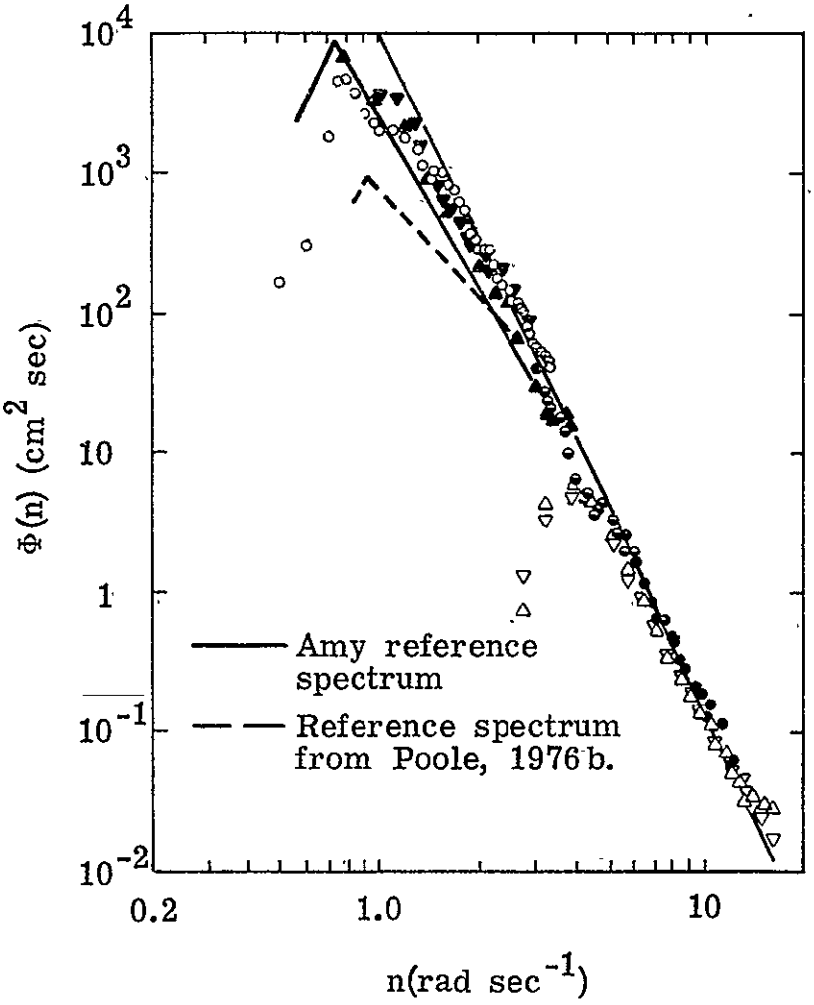

Figure 11.- Comparison of reference spectra with the frequency spectrum of wind generated waves in the equilibrium range. From Phillips (1968, page 113, figure 4.8).

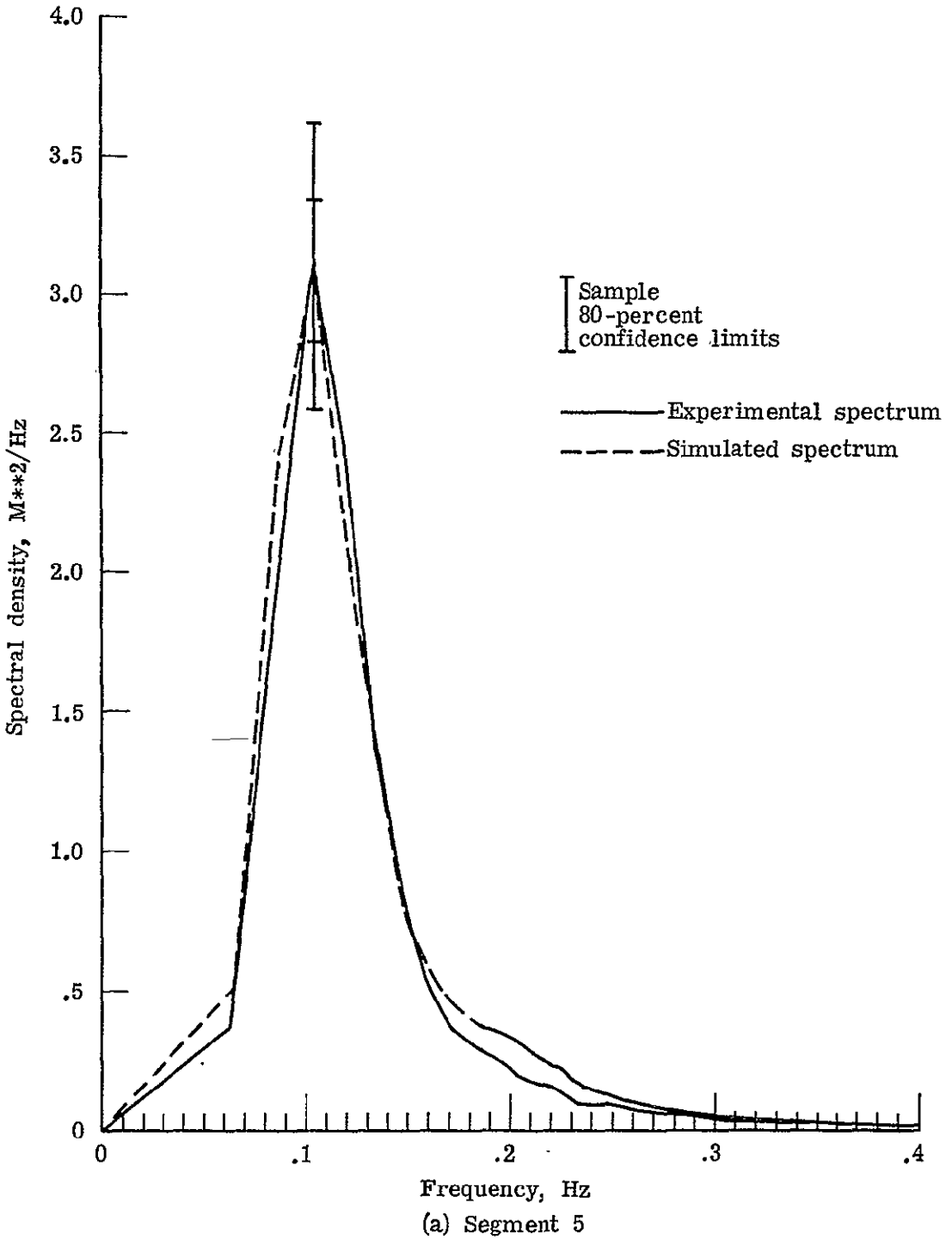

(a) Segment 5

Figure 12.- Comparison of experimental and simulated wave spectra for each data segment.

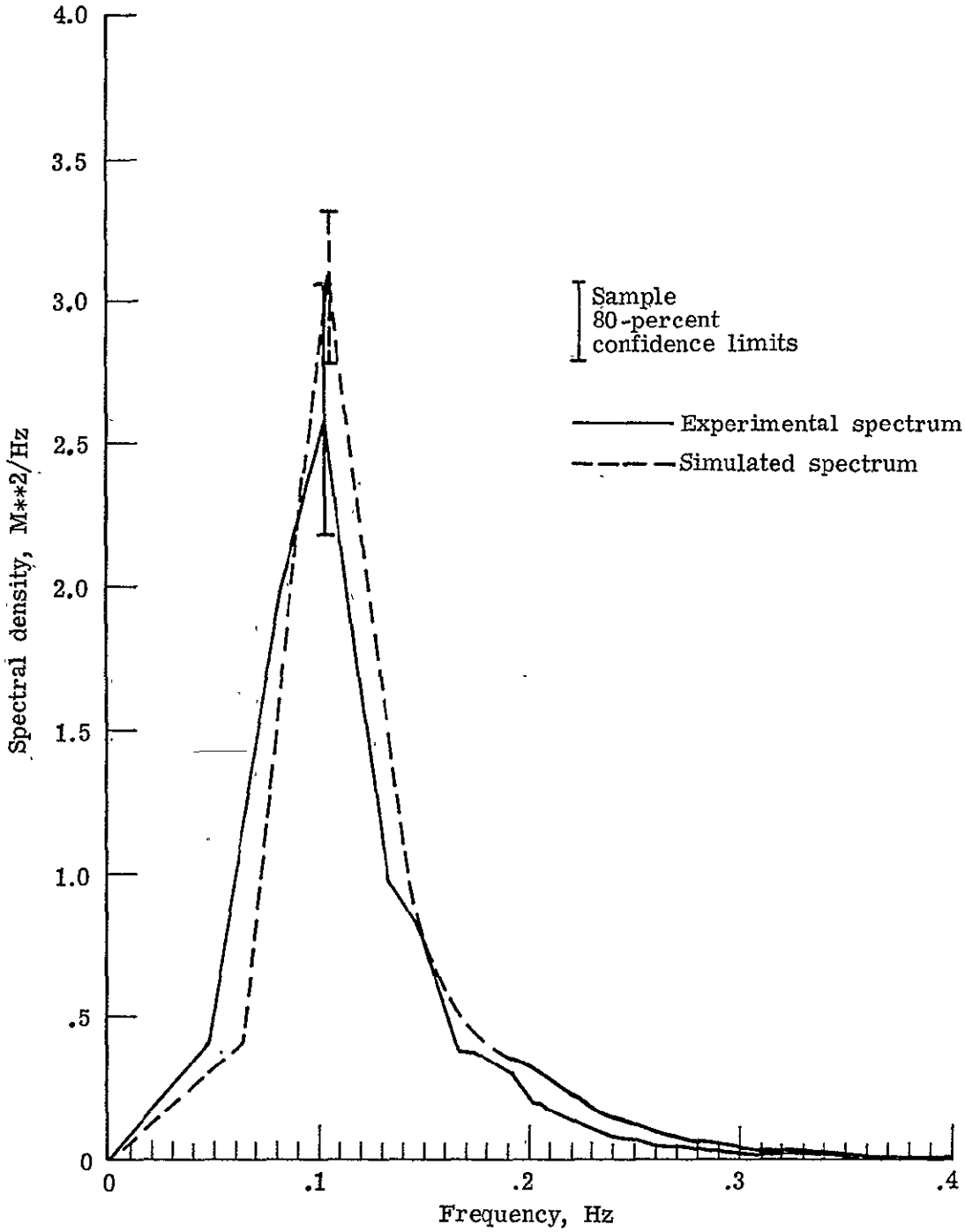

(b) Segment 6

Figure 12.- Continued

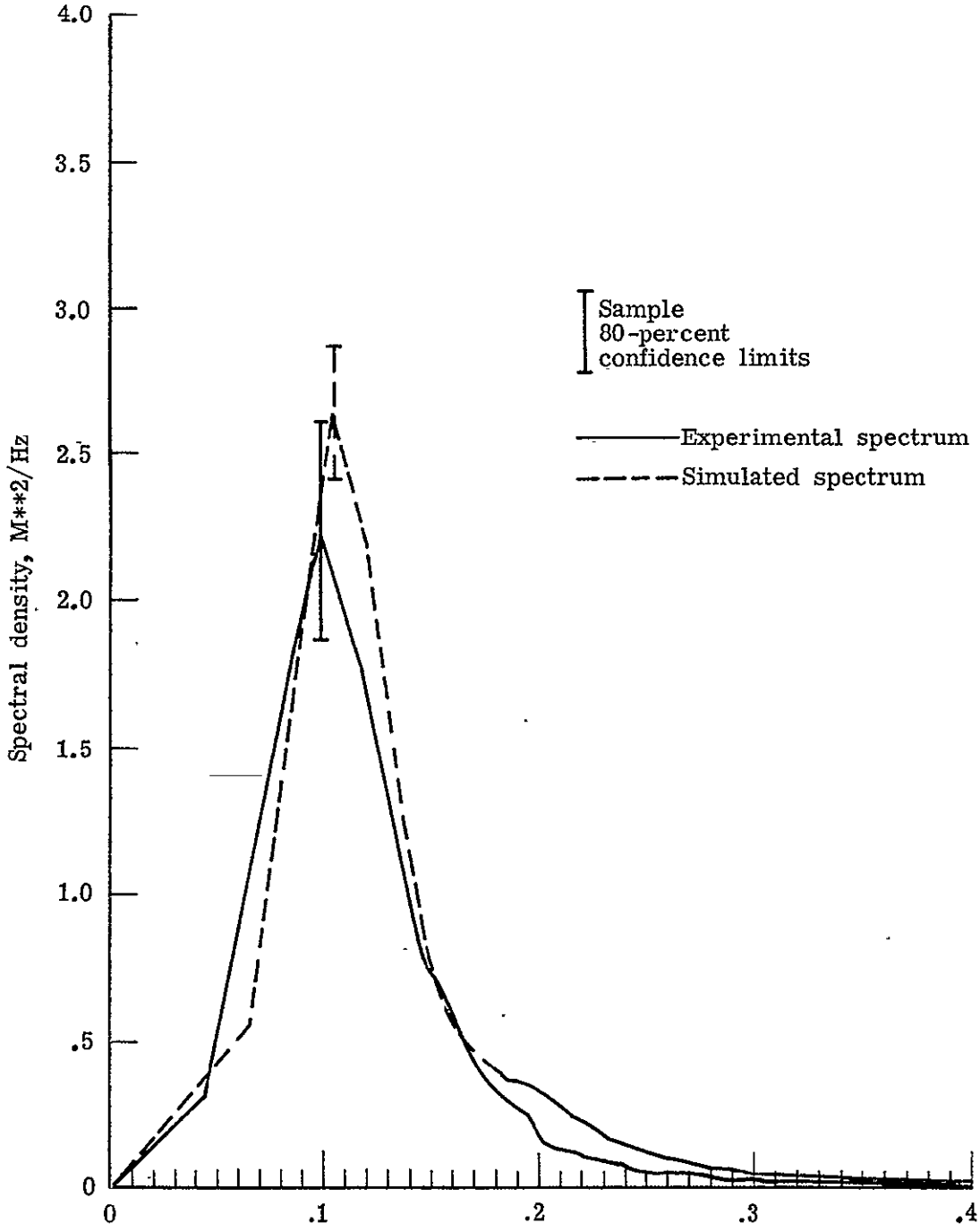

(c) Segment 7

Figure 12.- Continued

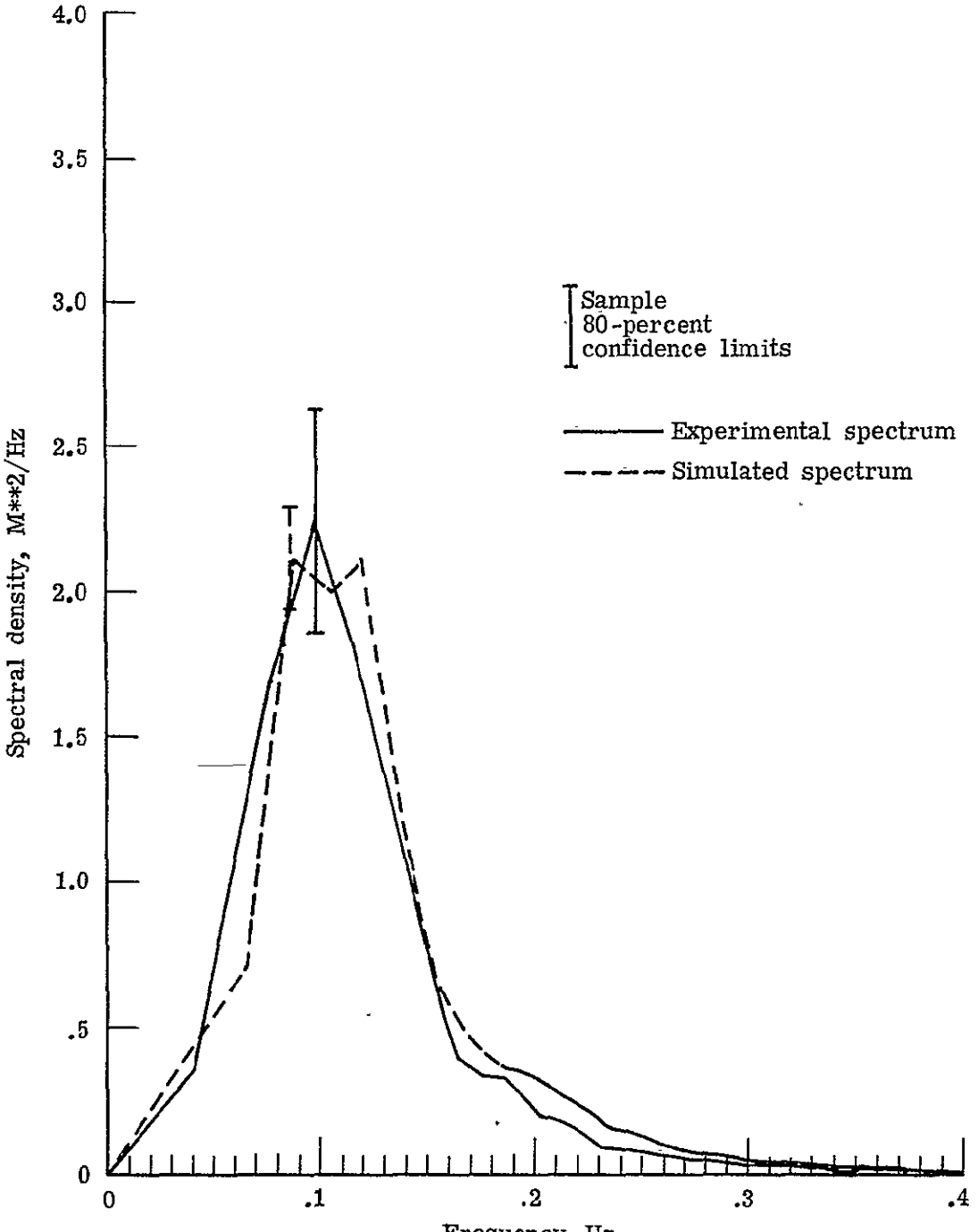

(d) Segment 8

Figure 12.- Continued

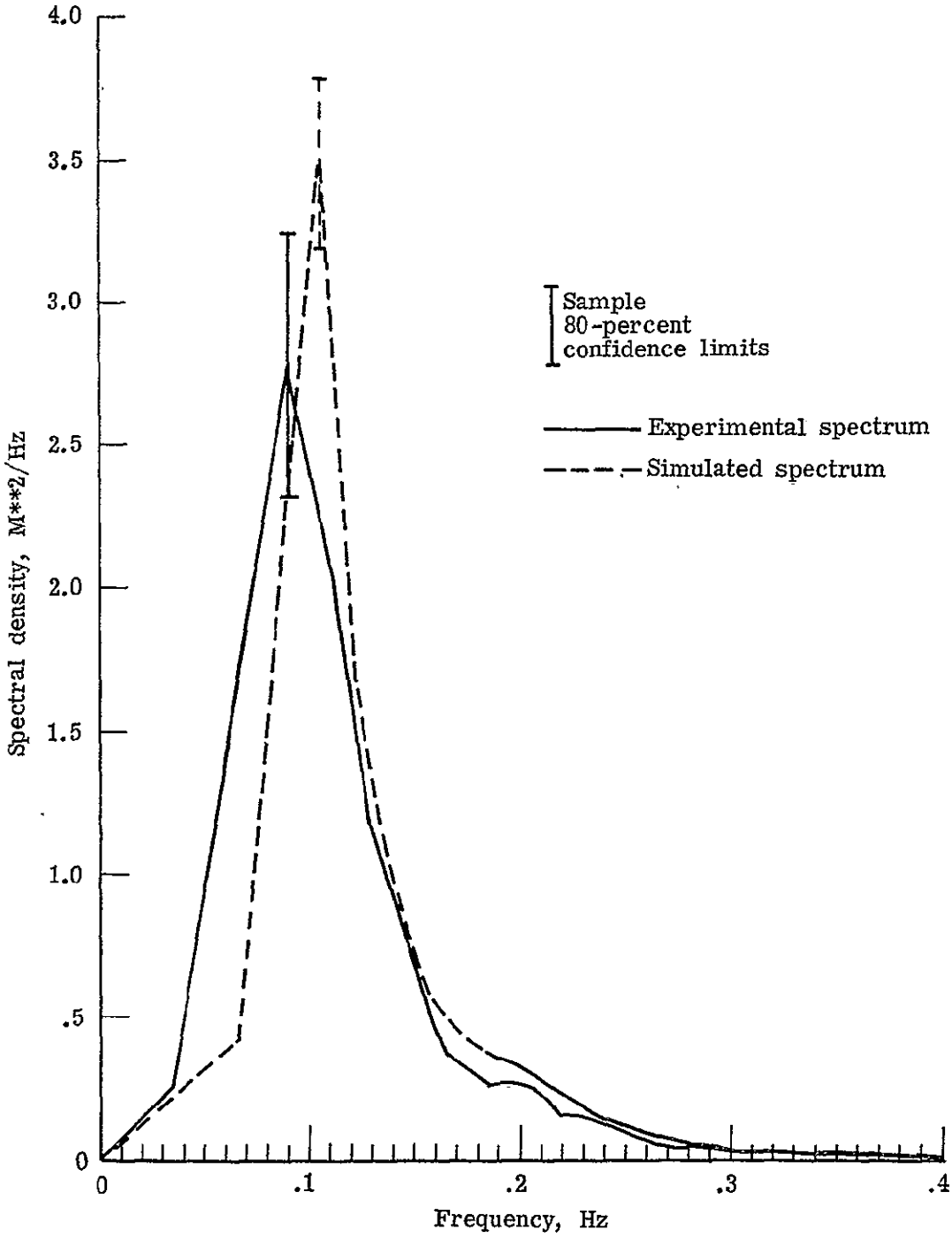

(e) Segment 9

Figure 12.- Continued

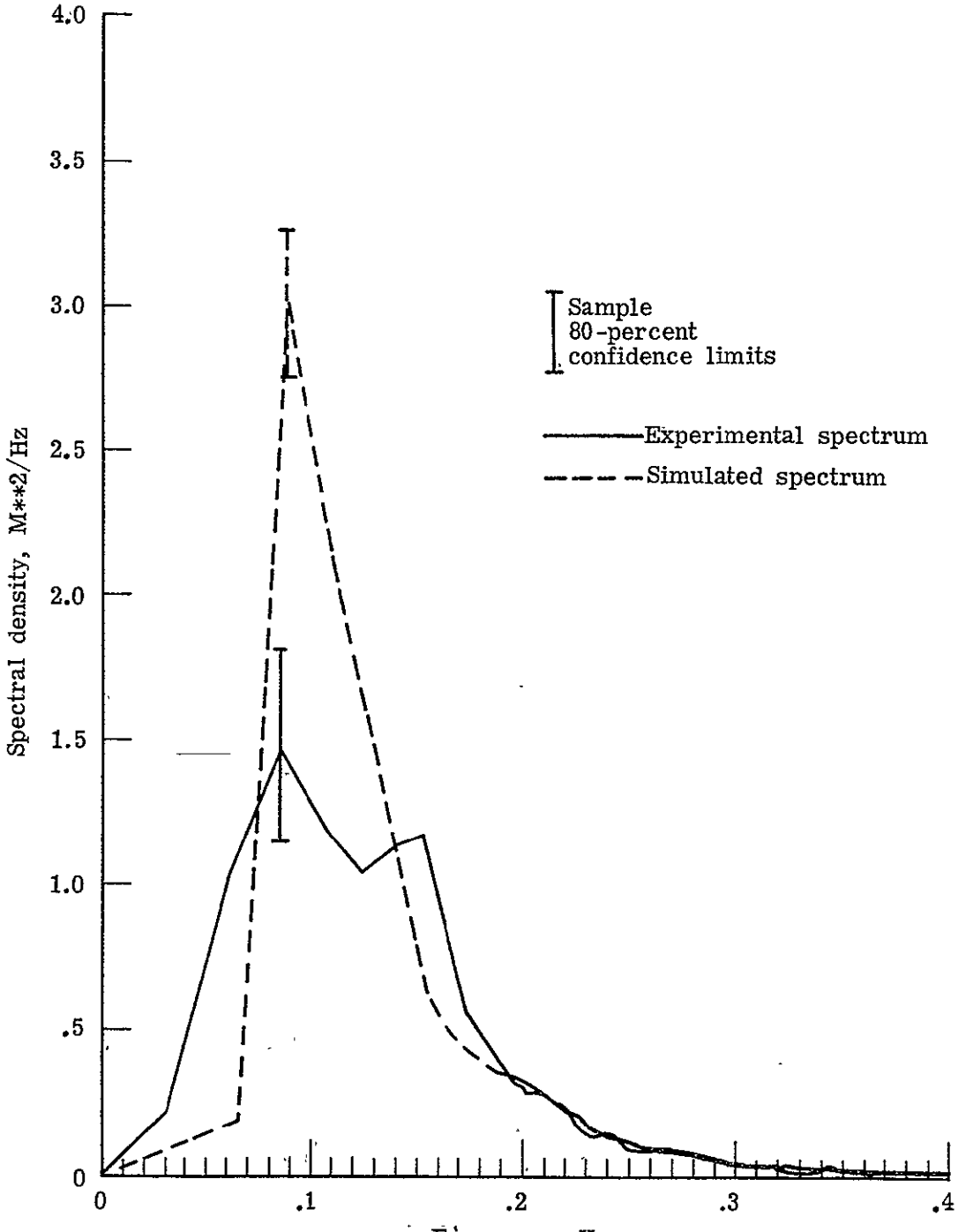

(f) Segment 10

Figure 12.- Concluded

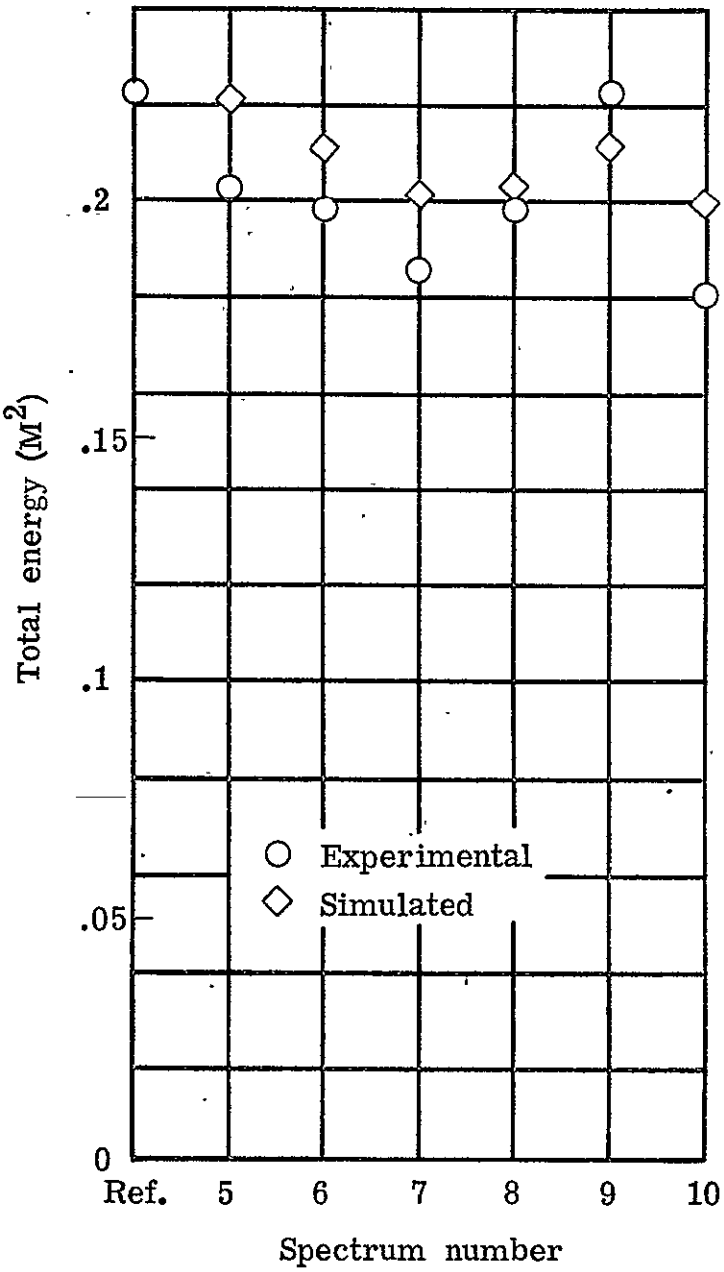

Figure 13.- Experimental and simulated total energy variation with data segment.

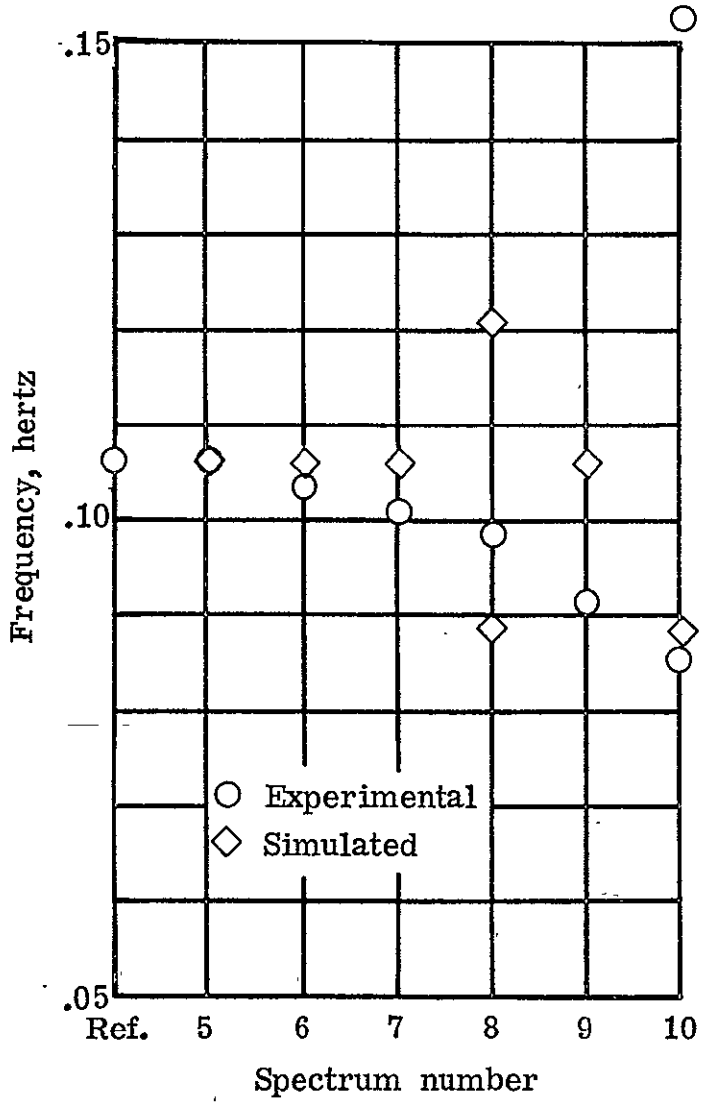

Figure 14.- Experimental and simulated frequency of peak spectral density variation with data segment.

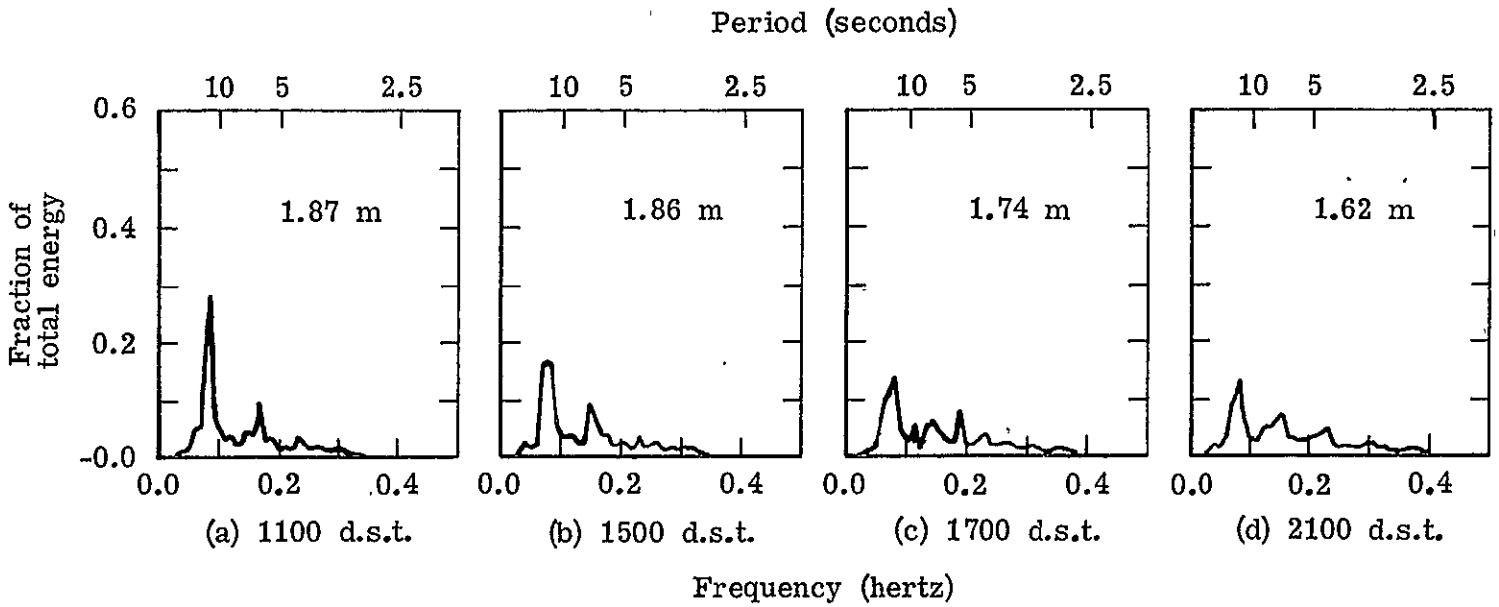

Figure 15.- Wave spectra from the CERC shore gauge at Jennette's Pier, Nags Head, North Carolina (Harris, 1975). Significant wave heights are shown for each spectra.

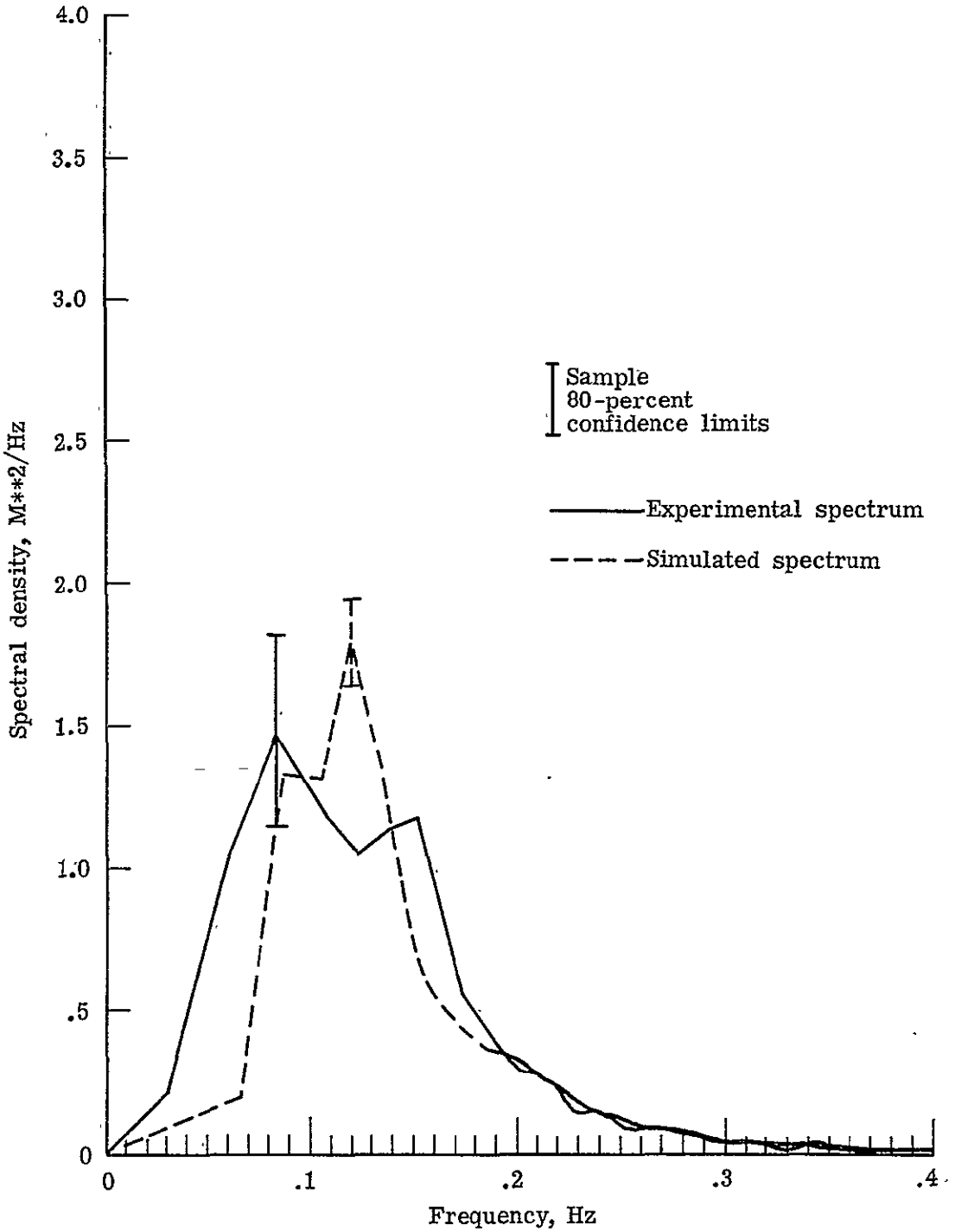

Figure 16.- Comparison of the experimental spectra of data segment 10 with the simulated spectra computed without energy from wave rays which formed "caustics".